INFLUENCE OF LOCAL PO_2 ON SKELETAL MUSCLE MICROVASCULAR BLOOD FLOW DURING HYPERINSULINEMIA

by © Brenda N Wells, BSc

A Thesis submitted to the School of Graduate Studies in partial fulfillment of the requirements for the degree of **Master of Science in Medicine (Cardiovascular Sciences)**

Division of BioMedical Sciences, Faculty of Medicine

Memorial University of Newfoundland

February 2022

St. John’s, Newfoundland and Labrador

Abstract

The goal of this thesis was to test the hypothesis that insulin mediated hyperemia is partially dependent on local muscle oxygen concentration. To do so, microvascular blood flow was measured in response to varying imposed concentrations of oxygen in rat skeletal muscle. Sprague-Dawley rats were anesthetized, and the extensor digitorum longus (EDL) was reflected onto an inverted microscope. Intravital video microscopy sequences were recorded during baseline and hyperinsulinemic euglycemia. The muscle was reflected over a glass stage insert (Experiment 1a and 1b), or over a gas exchange chamber (Experiment 2), and microvascular capillary blood flow was recorded during sequential changes (7%-12%-2%-7%) of oxygen (O_2) concentration. Blood flow was measured by the red blood cell supply rate (SR) in number of cells per second. In Experiment 1a, supply rate (SR) increased from 8.0 to 14 cells/s at baseline to euglycemia ($p = 0.01$), while no significant SR variation was detected after performing a sham hyperinsulinemic euglycemic clamp (Experiment 1b). In Experiment 2, SR decreased at 12% O_2 and increased at 2% O_2, compared to 7% O_2, under both experimental conditions. SR responses to oxygen square wave oscillations during euglycemia were not different to those at baseline at each O_2 concentration ($p > 0.9$). Our results suggest the increase in blood flow observed in response to insulin is eliminated if tissue oxygen microenvironment is clamped at given oxygen concentrations.

All animal protocols were approved by Memorial University's Institutional Animal Care Committee.

Keywords: microcirculation, oxygen transport, insulin, hyperinsulinemic euglycemic clamp, intravital video microscopy, capillary

General Summary

The goal of this thesis was to determine if blood flow increases caused by insulin are affected by oxygen levels. To do so, blood flow was measured in response to different levels of oxygen in rat muscle. A muscle located in the rat's leg was placed onto a microscope stage. The muscle was reflected over glass (Experiment 1a and 1b), or over a gas exchange chamber (Experiment 2), and blood flow was recorded across different oxygen levels. Live video recordings were taken during both normal and high insulin conditions. In Experiment 1a, blood flow was significantly faster in high insulin conditions compared to normal conditions. In Experiment 2, blood flow was slower at high oxygen levels and faster at low oxygen levels under both normal and high insulin conditions. Blood flow responses to changing oxygen levels were not different between normal and high insulin conditions. Thus, our results suggest that the increase in blood flow observed in response to insulin is eliminated if oxygen is held at a given oxygen level.

Acknowledgements

I would like to take the time to extend my appreciation and gratitude to those who have made this research project possible. Conducting the experiments within this thesis has been a challenging, but wonderful experience, and I couldn't have done it all on my own.

First, I would like to thank my fellow lab members for taking the time out of their busy schedules to help me with numerous tasks during my project. Hamza Shogan taught me how to perform a hyperinsulinemic euglycemic clamp, which was a critical piece in all of my experiments. Meghan Kiley assisted me when learning the necessary surgical techniques and helped me early on in my degree with data analysis and organization, as well as assisting me with many experiments throughout my project. Meaghan McCarthy assisted me with experiments throughout my degree as well. And finally, I would like to thank Gaylene Russell for continuously supporting me during almost every aspect of my project from start to finish. No matter how many questions I asked her, she was always eager to answer them; Gaylene took me in under her wing, and I truly wouldn't have succeeded without her.

Secondly, I would like to thank my committee members, Dr. Bruno Stuyvers and Dr. Reza Tabrizchi, for taking the time throughout my whole degree to help guide me with my project and give helpful advice where needed. Additionally, Dr. Stuyvers and Dr. Tabrizchi played a huge a role in reviewing and polishing my thesis in preparation for examination.

Thirdly, thank you to the Canadian Institutes of Health Research and the Faculty of Medicine at Memorial University of Newfoundland for funding support for this project. These funds made all of the work contained in this thesis possible.

Lastly, I send my sincerest thanks to my supervisor, Dr. Graham Fraser, who has been an incredible mentor to me since the day I became a graduate student in his lab. He has always been a kind and empathetic supervisor, who has also pushed me to be the very best version of myself. Dr. Fraser has helped me acquire a deep understanding of the microcirculation and skills that will continue to aid me throughout my career.

Table of Contents

List of Figures

Lists of Tables

List of Appendices

Abbreviations

10X	ten times magnification
3D	three-dimensional
ANOVA	analysis of variance
ATP	adenosine 5’-triphosphate
cAMP	cyclic adenosine monophosphate
CEU	contrast-enhanced ultrasound
CO_2	carbon dioxide
EDF	extended depth of field
EDL	extensor digitorum longus
EDRF	endothelium-derived relaxing factor
eNOS	endothelial-derived nitric oxide synthase
Hb	hemoglobin
HCO_3	bicarbonate concentration
IVVM	intravital video microscopy
L	path length
L-NMMA	L-NG-monomethyl arginine acetate
N_2	nitrogen
NO	nitric oxide
O_2	oxygen
OD	optical density
PCO_2	partial pressure of carbon dioxide

PO_2	partial pressure of oxygen
PDMS	poly(dimethylsiloxane)
RBC	red blood cell
ROS	reactive oxygen species
SAD	sum of absolute difference
SO_2	oxygen saturation
STI	space time image
TCO_2	total carbon dioxide
ε	molar attenuation coefficient

Co-Authorship Statement

This thesis is structured in 3 chapters. Chapter 1 provides background knowledge, chapter 2 is a manuscript that describes original research, and chapter 3 is a summary chapter.

This thesis contains the following manuscript that is in preparation:

BN Wells, GM Russell McEvoy, H Shogan, ME Kiley, GM Fraser.
Clamping skeletal muscle PO_2 eliminates hyperinsulinemic microvascular blood flow response. (In preparation for submission to *Microcirculation*)

The project was designed by BN Wells and GM Fraser.

Animal surgeries were completed by BN Wells and GM Fraser.

Gas exchange chamber was three-dimensionally (3D) printed by GM Russell McEvoy.

GM Russell McEvoy assisted in blood gas sampling contributing to Tables 2.1 and 2.2.

H Shogan assisted in refining the apparatus for insulin and glucose infusion during the hyperinsulinemic euglycemic clamp contributing to Figure 2.1.

ME Kiley assisted in organization of the data collected from the oxygen oscillations contributing to Figures 2.10 – 2.14.

Data collection, data analysis, interpretation of data, preparation of figures and the manuscript in the current thesis was completed by BN Wells with critical review by GM Fraser. Co-authors contributed to critical revision of the manuscript in preparation for submission.

Chapter 1: Introduction and Background

1.1 Objectives

The cardiovascular system is responsible for pumping and transporting blood and nutrients from the heart to every organ and tissue throughout the mammalian body. This system consists of a branching network of blood vessels, starting with large arteries, that facilitate high volume blood flow, and ending with the intricate microcirculation found in all tissues. Because of its relatively easy access, skeletal muscle is a suitable and well-documented model of tissue for the study of microcirculation.

The microcirculation matches the supply and demand of active or inactive skeletal muscle through dynamic regulation of the blood flow entering the capillaries - the smallest vessels of the vascular system where exchange of nutrients between blood and tissue occur. In skeletal muscle, regulation of blood flow entering the capillaries is conducted through the modulation of arteriolar diameter. Arterioles are blood vessels that precede the capillaries in the cardiovascular tree and whose walls contain smooth muscle which can constrict or dilate thus adjusting vascular resistance and flow. Numerous factors can influence arteriolar tone across a wide range of conditions, including high insulin levels and varying tissue oxygen concentrations, which contributes to modulate the rate of blood flow entering the microvasculature (Duling, 1974; Pittman & Duling, 1973; Richey, 2013; Steinberg et al., 1994). Oxygen, in addition to glucose, is also a requirement for aerobic respiration and ATP production within muscle tissue. Insulin has been shown to increase blood flow to the microcirculation through vasodilatory mechanisms and to increase the uptake of glucose into skeletal muscle (Akerstrom et al.,

2019; Ramos et al., 2020; Wang et al., 2013). Additionally, increased blood flow to the capillary bed, either dependently or independently of insulin, leads to an increase in the delivery of glucose to muscle tissue, which further increases glucose uptake and metabolism as the muscle is provided with more glucose that can be availed of (Balon & Nadler, 1997; Baron et al., 1994; McClatchey et al., 2019). Together, these factors support the existence of a connection between oxygen and insulin effects on blood flow response. This putative "oxygen-insulin" relationship has not been addressed to date and numerous questions remain.

In particular, the increase in the microvascular blood flow seen in response to insulin may not only to facilitate glucose uptake by delivering more glucose, but may also ensure the sufficient supply of oxygen to the muscle (Baron et al., 1994). To fill this gap in our understanding of how the regulation of microvascular blood flow is linked to insulin, I have tested the following hypothesis:

The blood flow responses to insulin are partially mediated by the local metabolic demand reflecting the increased oxygen consumption required to uptake and convert glucose into glycogen in skeletal muscle.

To test this hypothesis, I addressed the following objectives:

1. Experiment 1a was to verify in this model whether, as seen previously (Akerstrom et al., 2019), capillary blood flow increases under hyperinsulinemic conditions in skeletal muscle microcirculation when performing a hyperinsulinemia euglycemic clamp. The combination of the clamp with IVVM was used to show that both blood flow and glucose uptake increases in response to increased insulin levels.

2. Experiment 1b was to confirm that the hyperinsulinemic euglycemic clamp method is effective in studying insulin blood flow responses and glucose metabolism. I performed a sham hyperinsulinemia euglycemic clamp to verify that potential flow increases were a result from the euglycemic clamp and not from the effect of time or fluid infusion.
3. Experiment 2 was to combine a gas exchange chamber device with the hyperinsulinemia euglycemic clamp and, using IVVM, to study the combined effects of oxygen and insulin on blood flow. The gas exchange chamber setup was designed to enable rapid changes of local oxygen concentrations in the muscle tissue microenvironment while insulin and glucose are simultaneously being infused through the clamp method.

1.2 The Microcirculation

The mammalian circulatory system is a closed compartment that is responsible for carrying blood from the heart throughout the body through a branching network of interconnected blood vessels. Oxygenated blood is pumped from the heart through systemic arteries which continue to branch into progressively smaller vessels. The capillaries are the smallest vessels of the vascular tree and provide the exchange interface between the blood and surrounding tissues. Blood is drained from the capillaries into the venous vascular tree which transports blood back to the heart and lungs through the venous system to be reoxygenated. Thus, the microcirculation can be defined as the blood vessels with a diameter of less than 300 μm in humans and less than 100 μm in rats. Arterioles (diameter in human: 5 - 100 μm), capillaries (5 - 10 μm) and venules (8 - 100

μm) are the major constituents of the microcirculation (Popel and Johnson, 2005). These vessels form intricate and expansive networks through skeletal muscle, which enables dynamic and localized control of blood flow within the tissue.

Feed arteries supply blood to first-order arterioles (arterioles directly branching from an artery) that progressively branch distally into smaller arterioles of successive orders before eventually branching into terminal arterioles which immediately precede the capillary beds (Jackson, 2016). The wall of arteriolar vessels, which precede the capillaries in the cardiovascular tree, contain a collagen fibre coating, smooth muscle layer, a basement membrane, and an endothelium. The layer of smooth muscle cells allows the arterioles to constrict and dilate, hence modulating the rate of blood flow entering the downstream capillaries (which lack smooth muscle cells). Endothelial cells form the linings of the heart and every blood vessel across the entire cardiovascular tree and contribute to control the passage of materials in and out the bloodstream (Alberts, et al., 2002). These endothelial cells also play a crucial role in the modulation of smooth muscle cells. For example, the endothelial cells respond to physical changes in the vessel such as the shear stress generated by the blood flowing through the vessel, leading to changes in the arteriole diameter through modulation of smooth muscle tone. Similarly, the endothelium also responds to neural signalling by releasing various vasoactive agents that rapidly induce constriction or dilation of arteriolar smooth muscle, thus regulating the blood flow entering the capillaries downstream (Alberts, et al., 2002; Amiya, et al., 2014). Capillary networks that branch from arterioles, form a dense, mesh-like, 3D interconnected arrangement. This creates a structure with a large surface area that interweaves in close proximity to all tissues in the mammalian body. This proximity

minimizes the distance between capillaries and tissue, thus facilitating the transport by diffusion of materials such as oxygen into the tissue, providing the essential fuel for aerobic metabolism (Smith et al., 2019). Diffusion of O_2 from a capillary to tissue is governed by Fick's 1st law of diffusion, and radial O_2 diffusion flux can be determined by Krogh's O_2 diffusion coefficient, K_{O2}. Direct evaluation of O_2 diffusion is technically challenging as it requires *in vivo* determination of the diffusion coefficient, therefore only approximations from *in vitro* data are used, and more recently computational models incorporating *in vivo* data have been developed (Bateman, 2003; Fraser et al., 2012a).

Although the microcirculation generally plays the same role across the body, its structure varies to match specific functions of each organ and tissue (Augustin & Koh, 2017). For example, in the central nervous system, the microcirculation not only provides the brain with nutrients and oxygen, but also plays a significant role in protecting the brain through strict regulation at the capillary endothelial layer. The capillary networks found in the brain are comprised of a mesh-like lattice that are even more dense in structure compared to other parts of the body. This structure provides a number of capillaries reaching all areas of the brain to continually supply nutrients to use as energy, as brain lacks its own fuel reserve. It has been suggested that nearly every neuron in the brain is matched with a capillary to provide these essential nutrients. The endothelium of these capillaries simultaneously blocks harmful substances from leaving the bloodstream through the blood-brain barrier. These capillaries have a continuous endothelium lining with tight junctions that form a highly regulated barrier that limits what molecules can cross between blood and tissue. This protects the brain from being exposed to potentially harmful endogenous or exogenous substances (Cipolla, 2009; Augustin & Koh, 2017).

This contrasts the fenestrated or sinusoidal capillaries that have pores or gaps in the endothelial lining in filtering organs such as the liver or kidneys; these gaps allow for free exchange of materials from the blood (Augustin & Koh, 2017).

Skeletal muscle contains the most expansive capillary beds in the body. The capillaries are arranged longitudinally in between muscle fibres, whereas the terminal arterioles (preceding these capillaries) and post-capillary venules (found immediately downstream) are largely oriented transversally (Mendelson et al., 2021). In contrast to the lattice pattern seen in the brain microcirculation, the capillaries of skeletal muscle are arranged around the architecture of muscle fibres, which are generally columnar in shape and can be millimetres in length in small animals and several centimetres long in humans (Mendelson et al., 2021). The intricacies of the capillary networks allow for precise execution of different functions across the body's organ systems, including the ability to regulate blood flow to match tissue activity in skeletal muscle.

1.3 Blood Flow Regulation

The microcirculation, across all tissues, is responsible for delivering nutrients and hormones, such as oxygen and insulin, while simultaneously removing waste products such as carbon dioxide, produced from cellular processes (Duling & Berne, 1970; Segal, 2005). This tightly regulated transport of substances through the microcirculation matches the metabolic demand of the muscle tissue. It is also responsible for maintaining the systemic homeostasis through the regulation of glucose delivery and subsequent disposal in skeletal muscle. As explained in 1.2, blood flow in the microcirculation is mainly

regulated by changes in the diameter of arteriolar vessels in response to different vasoactive stimuli. In addition to vasoactive stimuli released from endothelial cells, arterioles respond to stimuli from local blood flow to either dilate or constrict to alter the blood flow entering the branching capillary network. For example, an increase in shear stress experienced by the vessel wall will cause the arteriole to dilate, leading to an increase in blood flow downstream. Thus, arterioles play a role in the distribution of blood flow to specific capillary networks in skeletal muscle tissue.

Under resting conditions, arterioles exhibit a basal level of vasoconstriction via sympathetic activation of α-adrenoreceptors on smooth muscle cells, which contributes to maintain the mean arterial pressure within physiological range (Joyner & Casey, 2014). When aerobic metabolism is stimulated in skeletal muscle during exercise, the arterioles vasodilate in response to signals thought to originate downstream from various metabolites released from endothelium, tissue, and RBCs (Davis et al., 2008). Several vasodilatory mechanisms act to promote increased blood flow during periods of higher metabolic demand, with nitric oxide being one of the most thoroughly described. Nitric oxide (NO) was first proven to be the endothelium derived relaxing factor (EDRF) responsible for vessel relaxation under multiple conditions in the 1980s. The NO-mediated vasorelaxation of arterioles is now a well-documented mechanism (Bauer & Sotníková, 2010). Through the comparison of effects from endothelial-dependent relaxants such as bradykinin and the biological activity of EDRFs through bioassays, three independent research groups came to the conclusion that EDRF was in fact NO (Ignarro et al., 1987; Palmer et al., 1987; Furchgott, 1988). NO release from the endothelium and subsequent increase of downstream blood flow occur in response to

mechanical signalling, such as increasing shear stress in the vessel wall (Wray et al., 2011), or to neural signalling, such as muscle sympathetic nerve activity during exercise (Katayama and Saito, 2019). Interestingly, the blood flow increase during exercise is abolished when blocking NO production by specific antagonists, suggesting the involvement of NO in the hyperaemic response (Wray et al., 2011). Other studies have suggested a link between the release of NO and metabolites that effect the regulation of blood flow in the microcirculation, such as insulin, glucose, and oxygen (Steinberg et al., 1994; Richey, 2013; Balon & Nadler, 1997; Higaki et al., 2001; Hirai et al., 2010).

Recent evidence has implicated a role of K+ channels in blood flow regulation. K+ channels located in the capillary endothelium can stimulate a vasodilatory response and increase the flow in active muscle tissue (Jackson, 2017). Cells of excitable tissue, like skeletal muscle, rely on the efflux of K+ through K+ channels to repolarize the cell during each action potential. An accumulation of K+ ions in the interstitium occurs during periods of increased activity. K+ channels located in capillary endothelium are exposed to this accumulation and transduce this signal into endothelial cell hyperpolarization that is transmitted upstream. This signal is transmitted through gap junctions between electrically coupled endothelial cells to arterioles to stimulate an increase in their diameter. This results in an increase in blood flow entering the capillaries downstream, matching the increase in metabolic demand of the active muscle tissue creating the signal, generating a feedback loop (Jackson, 2017).

As mentioned above, like exercise, hypoxic conditions can enhance the blood flow to skeletal muscle capillary beds in order to provide more oxygen to the muscle tissue and remove the excess of carbon dioxide (Duling & Berne, 1970). The opposite also occurs

during hyperoxic conditions, in which the supplying arterioles vasoconstrict to reduce the blood flow in the microcirculation (Gutterman et al., 2017; Segal, 2005; Jackson, 2016).

Arterioles generally vasodilate in response to low oxygen levels to match metabolic supply and demand in active muscle tissue, but arterioles can also further constrict to limit blood flow in an inactive muscle tissue. Interestingly, metabolites, such as AMP or adenosine, can override the sympathetic vasoconstriction normally seen in all arterioles, to direct blood flow to active skeletal muscle tissue — a phenomenon known as functional sympatholysis (Calbet & Joyner, 2010; Remensnyder et al., 1962; Roy & Secomb, 2014). Blood flow regulation in response to changing oxygen concentrations in the microcirculation is a dynamic process that involves many contributing factors that play a role in matching the supply to skeletal muscle with its demand.

There is a lack of clarity in the literature on how oxygen concentrations in skeletal muscle tissue is sensed. The mechanisms by which arterioles are stimulated to modulate their diameters to regulate downstream microvascular blood flow in response to changing oxygen are also unknown. Numerous studies have shown that the arterioles themselves were responsible for sensing low oxygen pressures, while others have recently suggested that oxygen sensing was linked to NO release (Pittman & Duling, 1973; Duling, 1974; Jackson, 1987; Jia et al., 1996). However, the previously proposed mechanisms do not provide the level of sensitivity and rapid time course needed to match the oxygen supply with the demand in muscle tissue (Ellsworth et al., 2016). Additionally, myoglobin has been previously identified as a temporary O_2 store in both cardiac and striated muscle and may play a potential role in regulating O_2 levels in hypoxia conditions. The P_{50} of myoglobin is 3.1 mmHg demonstrating a high affinity for O_2. In cardiomyocytes, there is

evidence supporting the role of myoglobin in facilitated transport of O_2 into the cell. However, the results found in rat skeletal muscle do not demonstrate the same findings. In these studies, myoglobin had no effect on O_2 consumption or ATP production rate (Kamga et al, 2012).

Release of ATP from red blood cells (RBCs) has been shown in recent years to be a potential sensor of oxygen concentration. RBCs release ATP when hemoglobin desaturates in response to low oxygen environments. Hemoglobin desaturation in RBCs causes activation of the G-protein Gi and adenyl cyclase which leads to increases of the cyclic adenosine monophosphate (cAMP). Protein kinase A and then cystic fibrosis transmembrane inductance regulator are activated, causing release of ATP from the RBC through the pannexin-1 channel (Ellsworth et al., 2016). Luminal ATP is then believed to produce vasodilatory effects through binding to the P2 class endothelial purinergic receptors that subsequently stimulate endothelium-derived hyperpolarizing factors (Ellsworth et al., 2016).

Direct infusion of ATP into skeletal muscle microvasculature leads to vasodilation upstream in the feed arterioles, resulting in an increase in perfusion in the muscle tissue (McCullough et al., 1997; Collins et al., 1998; Dora, 2017). ATP release from RBCs not only plays a role in sensing low oxygen conditions but may also regulate microvascular perfusion through arteriole vasodilation (Ellsworth et al., 1995). In muscle tissue regions experiencing increased aerobic metabolism, RBC-released ATP travel upstream to dilate arterioles and increase blood flow in areas of muscle tissue with decreased oxygen concentrations, thereby matching the demand of active skeletal muscle. It has also been demonstrated in human blood that increased insulin levels, similar to levels seen in

diabetic states, inhibit the ATP release from RBCs *ex vivo* in low oxygen conditions, possibly due to the hydrolysis of cAMP and reduced expression of the G protein observed with increased insulin (Hanson et al., 2009; Hanson et al., 2010; Sprague et al., 2011). The release of ATP in low oxygen conditions and the subsequent inhibition in diabetic states further supports the hypothesis that oxygen saturation dependent ATP release from RBCs regulates blood flow in the microcirculation to match metabolic demand of tissue, and this may also be linked to both oxygen and insulin levels present.

1.4 Insulin and Glucose Uptake

Insulin is a peptide hormone released from β-cells in the pancreas and plays an important role in maintaining normal blood glucose levels in the body. Glucose levels are sensed by the β-cells through binding with the membrane receptor GLUT2, which triggers a signal cascade leading to the release of insulin into the bloodstream (Fu et al., 2019; Kolka & Bergman, 2013). Insulin travels through the body's circulation and binds with insulin receptors expressed on the microvascular endothelium and is transcytosed into the interstitial space. Within the interstitium, insulin can then bind to the appropriate receptors on the cell membranes of myocytes and trigger the translocation of the GLUT4 transporter to the cell surface (Bhattacharya et al., 2007). GLUT4 is a high affinity glucose transporter and, once inserted into the cell membrane, facilitates the diffusion of glucose down its concentration gradient into the myocyte. As glucose enters the muscle tissue, it is metabolized via oxidative phosphorylation to produce ATP, or undergoes

other metabolic processes such as glycogenesis depending on the energy demand (Bhattacharya et al., 2007).

In addition to stimulating translocation of glucose transporters to the cell surface, insulin has also been shown to elicit a blood flow response in the microcirculation. Insulin acts on the endothelial-derived nitric oxide synthase (eNOS) through the PI-3 kinase pathway, which is present in the microcirculation endothelium, to produce NO - a potent vasoactive stimulus (Richey, 2013; Wang et al., 2013). As described above, NO is released from endothelial cells and acts to vasodilate arterioles by inducing relaxation of the smooth muscles surrounding the vessels, therefore increasing blood flow downstream (Figure 1.1). Insulin binds to the insulin receptors on the endothelial cells and activates eNOS to release NO, thus causing an increase in blood flow. This mechanism has also been supported by studies of blood flow in human subjects (Steinberg et al., 1994).

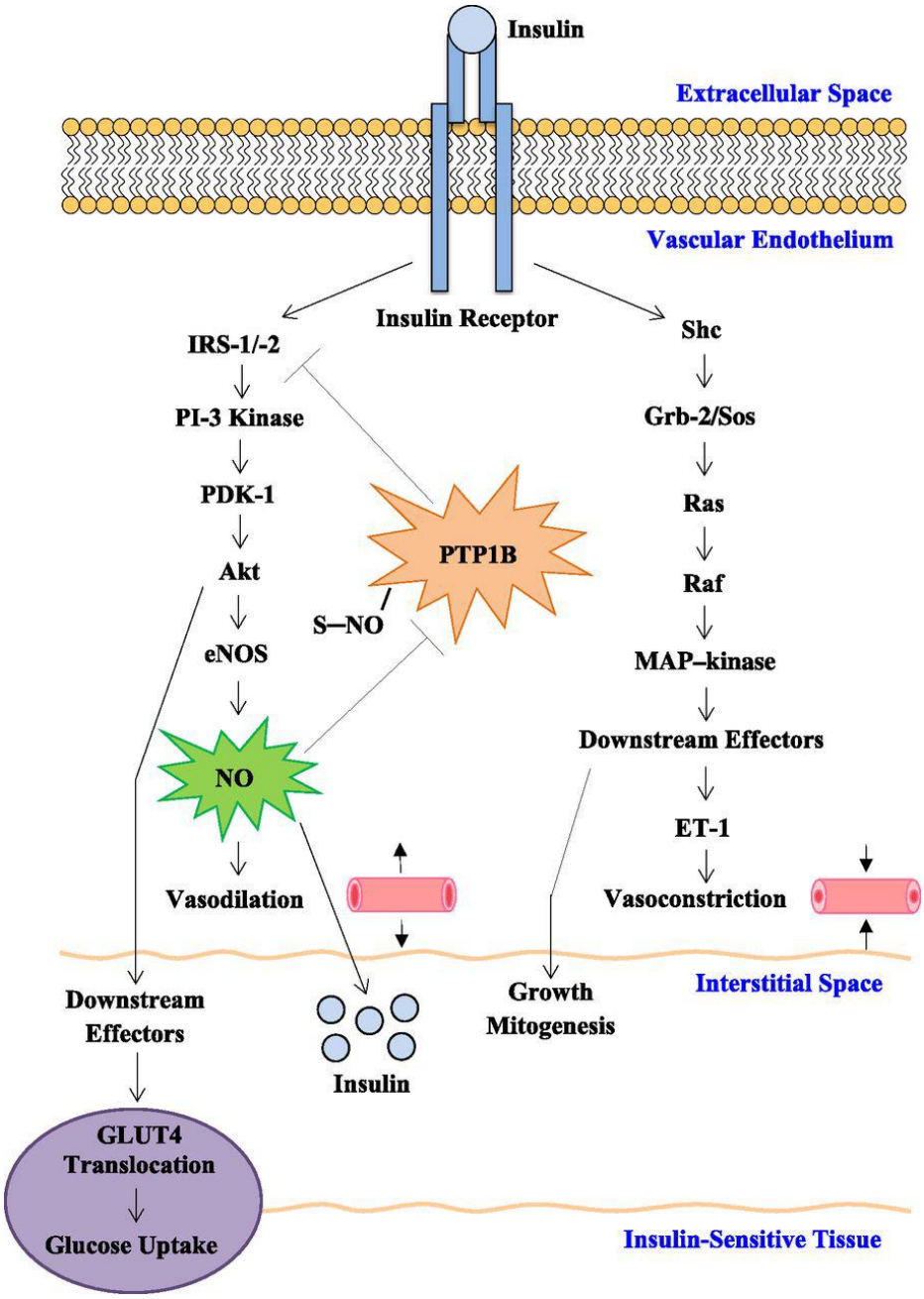
Insulin
Extracellular Space
Vascular Endothelium
Insulin Receptor
IRS-1/-2
PI-3 Kinase
PDK-1
Akt
eNOS
NO
Vasodilation
PTP1B
S—NO
Shc
Grb-2/Sos
Ras
Raf
MAP–kinase
Downstream Effectors
ET-1
Vasoconstriction
Interstitial Space
Downstream Effectors
Insulin
Growth Mitogenesis
GLUT4 Translocation
Glucose Uptake
Insulin-Sensitive Tissue

Figure 1.1 Insulin transduction pathway in endothelial cells. Insulin binds to its receptor on the endothelium layer resulting in the release of the vasoactive stimulus nitric oxide and translocation of the GLUT4 receptor to the cell surface in muscle tissue (Richey, 2013). (American Diabetes Association [The vascular endothelium, a benign restrictive barrier? NO! role of nitric oxide in regulating insulin action, American Diabetes Association, [2013]. Copyright and all rights reserved. Material from this publication has been used with the permission of American Diabetes Association.) https://diabetes.diabetesjournals.org/content/62/12/4006 Accessed August 26, 2021.

Insulin increases blood flow by dilating the arterioles and also stimulates GLUT4 translocation to the myocyte membrane. Therefore, insulin increases the supply of glucose to the skeletal muscle while simultaneously increasing the uptake of glucose in the muscle tissue through its increase of blood flow in the microcirculation.

It is well established that insulin plays an important role in regulating glucose concentration, however it is not the sole contributor (DeFronzo et al., 1979; James et al., 1985). Increases in blood flow separate from those seen from insulin binding have also been shown to increase the delivery of glucose to the skeletal muscle, and therefore lead to small increases in the uptake as well (Balon & Nadler, 1997; Higaki et al., 2001). NO, as described above, increases blood flow to the microcirculation by relaxing the smooth muscle of arteriolar vessels (Wang et al., 2013). This vasoactive stimulus can result in an increase in blood flow independently of insulin and leads to an increase in glucose uptake. Increase in the blood flow per se allows more glucose to reach the muscle tissue, and subsequently allows more glucose to be used for metabolic process in the skeletal muscle (McClatchey et al., 2019).

Glucose is the most efficient energy source for ATP production through oxidative phosphorylation in the muscle tissue under aerobic conditions, thus generating the energy needed by the muscle to perform normal cellular functions. Sufficient levels of oxygen in the microcirculation are also required for oxidative phosphorylation in the myocytes. Previous literature has suggested a potential link between oxygen concentrations in the microcirculation and glucose uptake into skeletal muscle because the biochemical

processes of both lead to production of ATP. One study suggested, through computational modelling, that the sensing of glucose is dependent on the oxygen concentration available to pancreatic tissue and suggested that a similar phenomenon occurs in muscle tissue as well (Wilson & Matschinsky, 2019). As mentioned previously, under normoxic conditions, glucose metabolism requires oxygen to produce ATP through aerobic respiration, therefore it would be reasonable to assume that sufficient levels of oxygen must be present in muscle tissue in order to uptake glucose for ATP production to occur. Reactive oxygen species (ROS), which are by-products of oxidative metabolism, have also been studied as a potential regulator of muscle glucose uptake. One study found that ROS, particularly H_2O_2, play an important role in contraction-mediated activation of glucose transport in fast-twitch muscle (Sandstrom et al., 2006). This is one of the few studies that suggest a potential link between glucose fixation and oxygen concentrations in the muscle tissue, independently of circulating insulin levels.

1.5 Hyperinsulinemic Euglycemic Clamp

A hyperinsulinemic euglycemic clamp is an experimental method frequently used to investigate a subject's overall sensitivity to insulin and the resulting glucose uptake rate. This method consists of simultaneously infusing insulin and glucose at rates based on animal weight and blood glucose concentration, with the achievement of euglycemia being the end point. Euglycemia is defined as the steady-state condition in which normal blood glucose level (between 5 - 7mM) is maintained through variable infusion of glucose in conjunction with steady insulin infusion (DeFronzo et al., 1979). During

hyperinsulinemic state, human or animal subjects are infused with a steady concentration of insulin while infusion of glucose is adjusted to achieve and then maintain euglycemia. The glucose infusion rate at euglycemia reflects the overall glucose uptake, primarily by the muscle tissues throughout the body, and can be used as an indicator of insulin sensitivity, and overall glucose metabolism (DeFronzo et al., 1979). As the insulin circulates and binds to the endothelium on skeletal muscle myocytes during the clamp procedure, there is an increase in GLUT4 expression on the cell surfaces, leading to higher uptake of glucose into the muscle. Higher glucose infusion rate is required to reach normoglycemic levels, indicating that more glucose is being transported into the muscle tissue. This represents an increase in glucose metabolism, as more glucose is needed to be infused in order to maintain euglycemia as the insulin levels increase in the body (DeFronzo et al., 1979).

This quantification method of insulin sensitivity has been used in a variety of studies of insulin resistance in cardiovascular and metabolic research. The hyperinsulinemic euglycemic clamp is an effective method for comparing differing blood flow effects and metabolic deficits between healthy and diseased models (DeFronzo et al., 1979). Particularly, the blood flow response to an increase of insulin levels can be compared between healthy and insulin resistant models (DeFronzo et al., 1979); these changes in blood flow can be measured at different levels of the cardiovascular tree, including both larger arteries and the microcirculation (Bradley et al., 2019; Akerstrom et al., 2019). The clamp method also allows researchers to examine the effects of compounds, such as the widely studied drug metformin, on re-establishing the normal blood flow response to insulin in diseased models (Bradley et al., 2019). Other researchers have used the clamp

method in animal studies to examine the heterogeneity of insulin action in different skeletal muscle tissue throughout the body. It has been shown that insulin-induced increases in glucose disposal occurred primarily in muscles containing mostly oxidative fibres (James et al., 1985). In conscious rats, the rate of glucose uptake in glycolytic muscle was more than double the rates measured in oxidative muscles within the physiological range of circulating insulin levels. Aerobic respiration, a process that uses both oxygen and glucose, occurs mainly in these oxidative muscles and in much less extent in glycolytic muscles (James et al., 1985). This suggests a potential interaction between oxygen and insulin-mediated glucose uptake, as the glucose disposal occurred primarily in muscles where oxygen is being utilized under hyperinsulinemic conditions. This occurred despite oxidative and glycolytic muscles having similar oxygen consumption rates under resting conditions (Bockman, 1983).

The hyperinsulinemic euglycemic clamp method has also been used to study the pathways and mechanisms of insulin-mediated blood flow responses and glucose uptake in human (Clerk et al., 2006). Recently, the insulin pathway, specifically the phosphorylation of Akt, and glucose uptake in leg skeletal muscle was compared between lean and obese human volunteers. It was determined that there were no significant differences in the phosphorylation of Akt between groups, despite the obese individuals having reduced glucose uptake (Ramos et al., 2020). Additional research involving healthy and diabetic volunteers have used the clamp method to determine whether hyperinsulinemia impairs NO release from the endothelium in arterioles (Mahmoud et al., 2016). Hyperinsulinemia increased the expression of the vasoconstrictor endothelin-1, while simultaneously decreasing phosphorylation of eNOS resulting in a decrease in NO

production. This imbalance in vasoactive stimuli leads to increased basal vasoconstriction of the arterioles (Mahmoud et al., 2016).

A direct correlation between skeletal muscle capillary density and insulin-mediated glucose uptake has also been demonstrated in previous studies using the clamp method on human participants (Lillioja et al., 1987; Hedman et al., 2000). Additional studies have shown reduced capillary density and microvascular blood flow in diabetic subjects, meaning a decrease in delivery of glucose to skeletal muscle (Kindig et al.,1998). Furthermore, researchers using the clamp method demonstrated that muscle glucose uptake relies on the delivery of glucose to the muscle tissue, and this would likely be impaired in conditions that cause reduced capillary density and flow in skeletal muscle vasculature (Baron et al., 1994). In these studies, hyperinsulinemic euglycemic clamps have provided further insight into the relationship between insulin and glucose uptake, however oxygen concentration was not considered when discussing increased glucose uptake. In addition, many of these clamp experiments have been conducted on human participants and the microcirculation was not assessed directly.

1.6 Intravital Video Microscopy

Intravital video microscopy (IVVM) has become the standard method for studying blood flow in the microcirculation. It allows for the direct observation of blood flow compared to other methods, such as contrast-enhanced ultrasound (CEU), that indirectly measure blood flow (Akerstrom et al., 2019, McClatchey et al., 2020). The CEU method is based on the ultrasound imaging signal obtained from infused microspheres or

microbubbles that are intended to represent RBC flow in the capillaries. However, these microspheres or microbubbles are not the same size as RBCs and therefore do not accurately reflect actual RBC or plasma flow through the microcirculation due to size dependent differences in rheology (Akerstrom et al., 2019).

In the present thesis, IVVM was used to examine the microcirculation of the extensor digitorum longus (EDL) muscle of rats, a muscle preparation specifically developed for this approach. In this preparation, the muscle is carefully exposed by surgical technique and arranged on the stage of an inverted microscope for visualization of the microcirculation. A major advantage of the EDL preparation is the minimal mechanical manipulation of the muscle, therefore little, if any, damage is done to the muscle of interest if the method is performed correctly and the microvascular blood flow is not impacted and remains stable for many hours (Tyml & Budreau, 1991). Another advantage of this muscle preparation is that the EDL does not required to be bathed in a prepared superfusion fluid after exposure; it can instead be isolated from the surroundings using various approaches (Tyml & Budreau, 1991). Further, additional studies have confirmed that exteriorization of skeletal muscle does not affect vascular function (Bailey et al., 2000; Lindbom et al., 1982.; McClatchey et al., 2020). Other muscle preparations used for visualizing the microcirculation, such as the spinotrapezius and cremaster muscles, do not possess the same advantages as the EDL preparation as they are much thinner preparations. These thinner muscles may not be representative of typical fusiform skeletal muscle, especially larger muscles used for locomotion that possess extensive microvascular networks comprising of multiple capillary units used to facilitate blood flow regulation in active muscle tissue (Akerstrom et al., 2019; Mendelson et al., 2021).

Specifically, the EDL preparation readily allows for visualization of the structure of microvessels organized around the muscle fibres.

The IVVM method and apparatus used in the current thesis enabled the analysis of both hemodynamic parameters and oxygen saturation of RBCs flowing through capillaries. To measure hemodynamic parameters in the microcirculation, analysis of the IVVM video recordings can be conducted based on changes in light intensities of the video pixels in each recording. As mentioned above, most capillaries contain single-file RBC flow, therefore differences in light intensity can be identified between the RBCs flowing through the vessel and the distinct intermittent plasma gaps that were present. The fluctuating changes in light intensity are processed by a computer to generate space-time images (STIs), which describe the transit of RBCs over time and the position within the capillary lumen (Ellis et al., 1992). These images are then used to determine hemodynamic parameters such as RBC velocity (μm/s), which is calculated by tracking the displacement of RBCs across the capillary over a period of time. Lineal density (cells/mm) is determined by the number of RBCs per unit length along the capillary. RBC supply rate (cells/s) is the product of velocity and lineal density, and hematocrit is the ratio of RBC volume to the total measured volume of a vessel segment based on the measured vessel diameter (Figure 1.2).

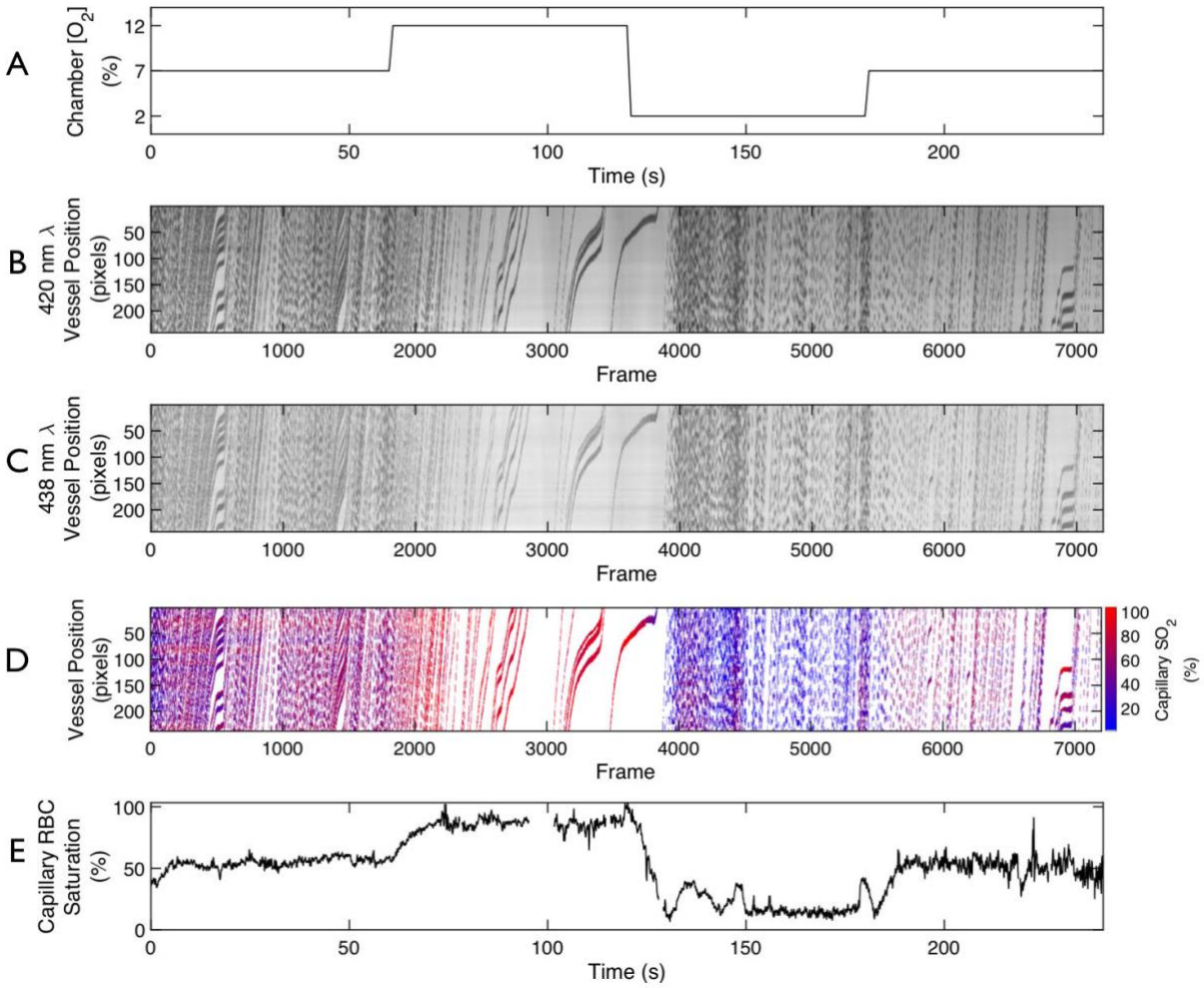
A
Chamber [O2] (%)
12
7
2
0
50
100
150
200
Time (s)
B
420 nm λ Vessel Position (pixels)
50
100
150
200
0
1000
2000
3000
4000
5000
6000
7000
Frame
C
438 nm λ Vessel Position (pixels)
50
100
150
200
0
1000
2000
3000
4000
5000
6000
7000
Frame
D
Vessel Position (pixels)
50
100
150
200
0
1000
2000
3000
4000
5000
6000
7000
Frame
100
80
60
40
20
Capillary SO2 (%)
E
Capillary RBC Saturation (%)
100
50
0
0
50
100
150
200
Time (s)

Figure 1. 2 Offline analysis conducted using custom MATLAB software to measure capillary RBC saturation. Saturation measurements were analyzed from selected capillaries during the imposed oxygen oscillations within the microcirculation of the extensor digitorum longus (EDL) muscle. A) The imposed oxygen oscillation performed during the 4 minute recording. Oxygen saturation of hemoglobin is calculated based on the ratio of the optical density measured from the isosbestic wavelength (420 nm) shown in B) and the oxygen-dependent wavelength (438 nm) STI shown in C). D) The optical density at each wavelength is measured using the light intensity of incident light and light intensity from RBCs flowing single-file through capillaries with clear plasma gaps in between. The lines in these images represent the transit of individual RBCs through the selected capillary throughout the 4 minute recording. E) RBC SO_2 of a selected capillary across the oxygen oscillation.

Oxygen saturation measurements involve the quantification of the absorbance of RBC at two different wavelengths while recording the microscopic fields — both an isosbestic (a specific point in which two chemical species have the same absorptivity) and oxygen-dependent wavelength (Ellis et al., 1990). For the isosbestic wavelength (e.g. 420nm), light absorption of hemoglobin is insensitive to changes in oxygen saturation because the molar attenuation coefficient is the same for both oxy- and deoxy-hemoglobin. The oxygen-dependent wavelength (e.g. 438nm) on the other hand is sensitive to changes in oxygen saturation. This wavelength corresponds to a disparate light absorption, which is dependent on the relative oxy- and deoxy-hemoglobin concentrations (Figure 1.3). Thus, optical density measurements of RBCs taken at both wavelengths, as well as the combination of the two together, are necessary for measuring oxygen saturation of RBCs in the microcirculation, as seen in the calculation below, where the optical density (*OD*) at each wavelength is calculated from the length of the capillary (*L*) and the molar attenuation coefficient (ε) (Ellis et al., 1990; Ellsworth et al., 1987).

$$OD = \log\left(\frac{Io}{I}\right)$$

$$OD = L[Hb]\varepsilon$$

$$\frac{OD_{438}}{OD_{420}} = \frac{\varepsilon_{438}}{\varepsilon_{420}}$$

Oxygen saturation of hemoglobin is calculated based on the ratio of the optical density measured from the oxygen-dependent wavelength, divided by the isosbestic wavelength (Ellis et al., 1992). The optical density at each wavelength is measured using the light intensity of incident light and light intensity from RBCs (Figure 1.4). This is a

convenient measurement in capillaries because most of these vessels have single-file RBC flow, which creates distinct plasma gaps that can be used to measured incident light intensity. A linear relationship exists between the ratio of optical density measured from the two wavelengths and the RBC oxygen saturation – this is an adaptation of the Beer-Lambert's Law and allows for the spectrophotometric determination of microvascular RBC oxygen saturation (Ellis et al., 1990; Ellsworth et al., 1987). Both *a* and *C* are constants determined from *in vivo* calibration.

$$SO_2 = a\left(\frac{OD_{438}}{OD_{420}}\right) + C$$

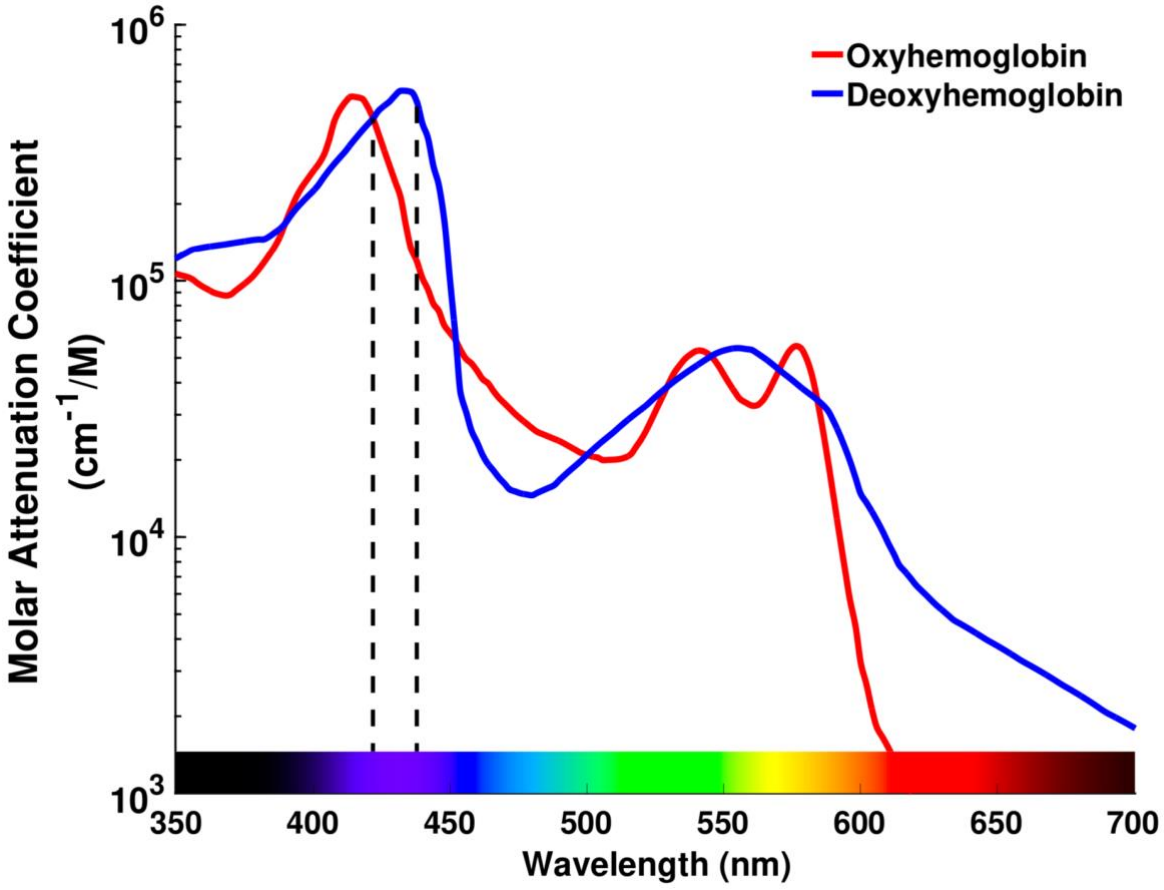

Figure 1. 3 Molar attenuation coefficients of hemoglobin. The difference in molar attenuation coefficient for oxy- (red line) and deoxy- (blue line) hemoglobin are shown across the visible spectrum as depicted by the horizontal colour bar. In the present thesis, were 420 nm and 438 nm wavelengths which are used for the calculation of red blood cell oxygen saturation (Adapted from Fraser, 2012, using data from Prahl, 1999).

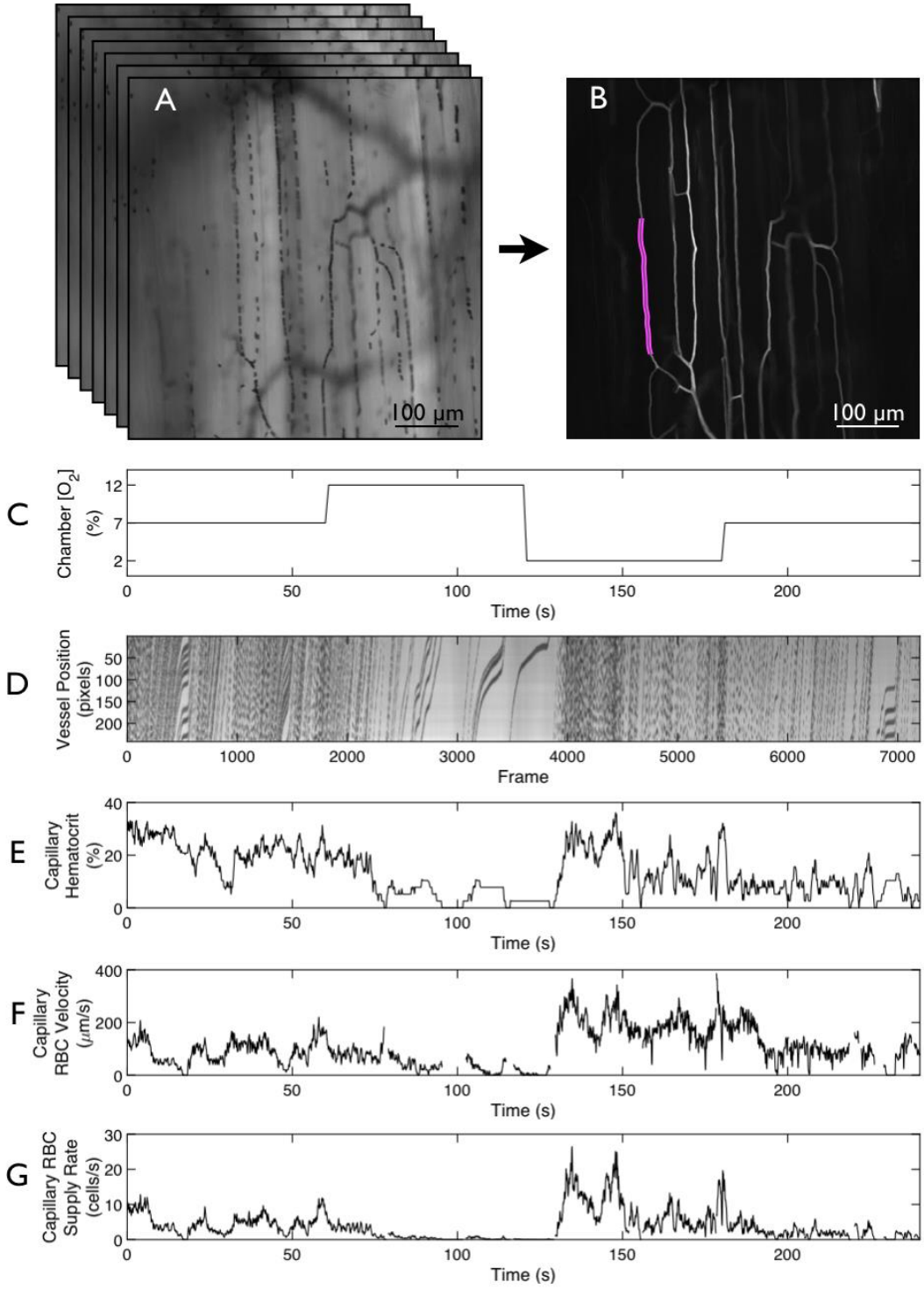
A
100 µm
B
100 µm
C
Chamber [O2] (%)
12
7
2
0
50
100
150
200
Time (s)
D
Vessel Position (pixels)
50
100
150
200
0
1000
2000
3000
4000
5000
6000
7000
Frame
E
Capillary Hematocrit (%)
40
20
0
Time (s)
F
Capillary RBC Velocity (µm/s)
400
200
0
Time (s)
G
Capillary RBC Supply Rate (cells/s)
30
20
10
0
Time (s)

Figure 1.4 Offline analysis conducted using custom MATLAB software to measure hemodynamics. Hemodynamic parameters were analyzed from selected capillaries during the imposed oxygen oscillations in the microcirculation of the extensor digitorum longus (EDL) muscle. A) Microcirculation is imaged by 4 minutes video sequences captured at 30 frames/sec, (7200 frames/video sequence). B) Perfused capillaries with single-file RBC flow are selected from functional images using a semi-automated process. These images are processed from the intravital microscopy recordings of different fields of view of the EDL microcirculation captured in real-time and display all of the perfused capillaries in a single field of view. C) The imposed oxygen oscillation in the gas exchange chamber performed during the 4 minutes recording. D) Light intensity fluctuations from plasma gaps between RBCs are used to generate space-time images (STIs), which are then used to calculate the hemodynamic parameters. The lines represent the transit of each RBC through the selected capillary throughout the duration of the 4 minute recording. E) Hematocrit of a selected capillary across the duration the oxygen oscillation. F) RBC velocity of a selected capillary across the oxygen oscillation. G) RBC supply rate of a selected capillary across the oxygen oscillation.

1.7 Gas Exchange Chamber

The gas exchange chamber is a recently developed 3D printed device that allows for the direct manipulation of skeletal muscle tissue environment (Figure 1.5) (Sové et al., 2021).

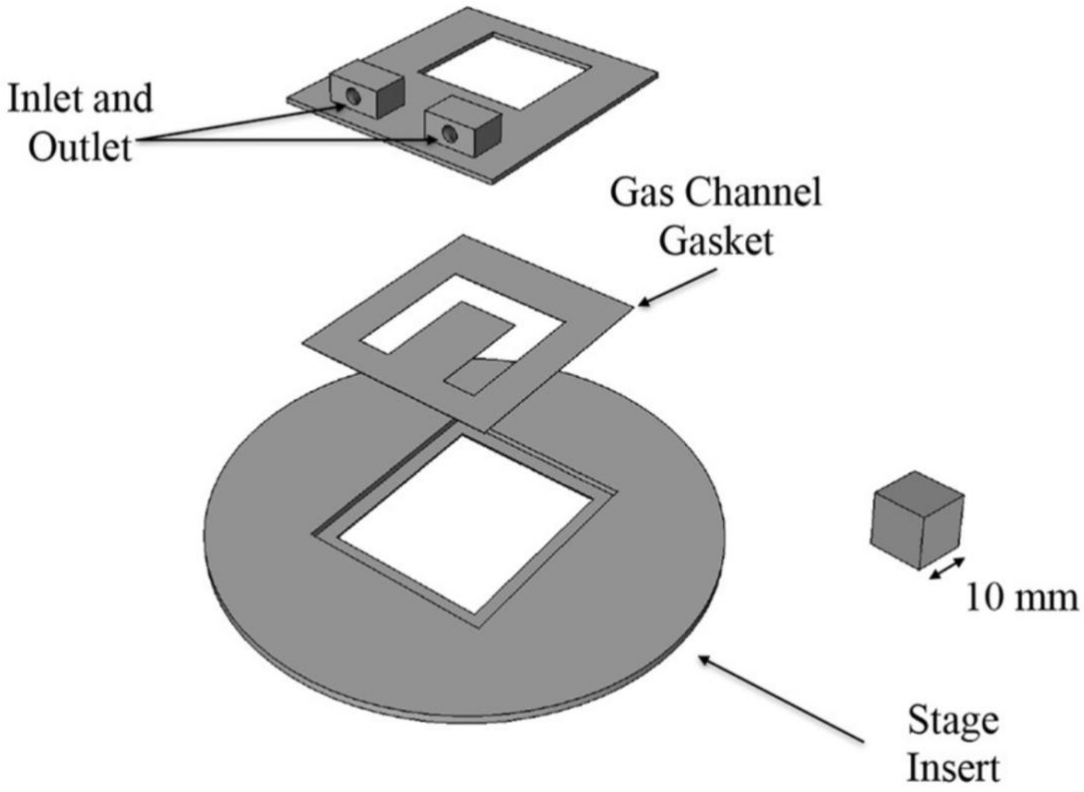

Figure 1.5 Three-dimensional (3D) computer aided design rendering of gas exchange chamber components. Components were 3D printed and the gas channel is sealed on the bottom with a glass cover slide (Sové et al., 2021, used under Creative Commons License).

This device is placed into the stage of the inverted microscope used for intravital microscopy and produces rapid changes in the muscle's tissue microenvironment that can be observed in real time within approximately 3s. The isolated EDL muscle is placed atop a thin poly(dimethylsiloxane) (PDMS) membrane, which is gas permeable, while simultaneously being covered by a thin impermeable film, resulting in the muscle being exposed only to exogenous gases flowing through a channel underneath the PDMS membrane (Figure 1.6).

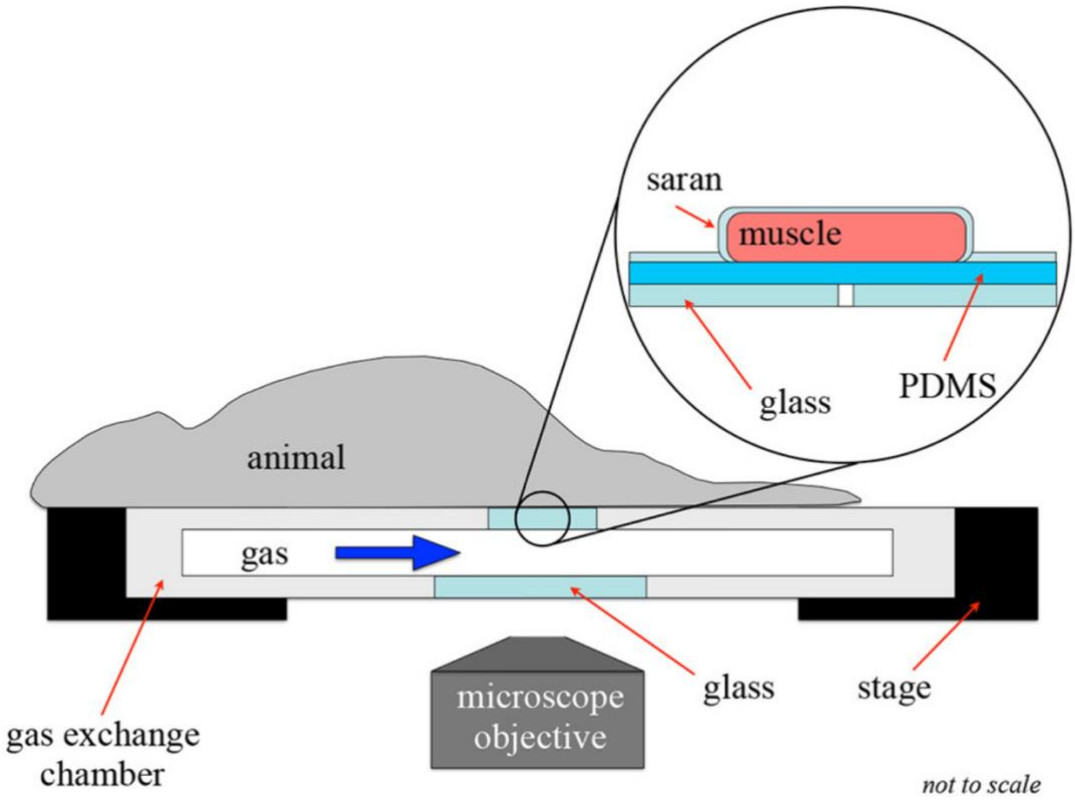

Figure 1.6 Experimental setup of the animal placed atop the gas exchange chamber. The gas exchange chamber insert is fitted into the microscope stage, with the muscle aligned over the PDMS membrane and covered with a small piece of gas impermeable polyvinylidene film (Saran, Dow Corning), therefore the muscle is affected only by the gases flowing through the chamber (Sové et al., 2021, used under Creative Commons License).

Gas exchange between the chamber and the muscle is facilitated by a gas permeable membrane made from PDMS allowing oxygen concentrations within the muscle to be manipulated dynamically. PDMS is ideal to facilitate this gas exchange because it is an elastomer that is permeable to gases due to its porous structure, it's an inexpensive material and is also optically transparent (Sové et al., 2021). The composition of gases flowing through the device and the PDMS are controlled using computer software connected to digital mass flow meters, which accurately measures the mass flow rate of the gases as they flow from their respective tanks to the gas exchange chamber. For example, skeletal muscle can quickly be perturbed to undergo hypoxic conditions by flowing a low oxygen gas composition through the gas exchange device, or vice versa with high oxygen concentrations in the exchange chamber.

Previously, superfusion fluids have been used with similar preparations to maintain the viability of the skeletal muscle being imaged. Superfusion consists of buffering a solution to immerse skeletal muscle that preserves the physiological state of the muscle. This solution could also be used to administer drugs to the muscle, making it an effective method for studying muscle vasculature. One aspect of preparing the superfusion fluid is bubbling the solution at a chosen gas composition, using some combination of nitrogen, carbon dioxide, and oxygen; therefore, when the muscle is bathed in this solution, the muscle tissue environment is held at the chosen gas concentrations, similar to how tissue gas concentrations are imposed using the gas exchange chamber. Some studies have examined the microcirculation of different skeletal muscle preparations that have been superfused in a solution with 95% N_2/5% CO_2, completely lacking oxygen (Williams, et al., 2018; Hirai, et al., 2010). It has been well established that muscle tissue needs oxygen

for metabolic purposes, including aerobic respiration to produce ATP, and immersing the muscle in a solution with 0% O_2 for a period of time will cause blood flow to the muscle to increase in order to supply the needed oxygen; therefore, the blood flow measurements gathered from such studies may be impacted by the chosen oxygen concentrations that the muscle tissue is exposed to. Using the gas exchange chamber, gas concentrations, most notably oxygen, are kept within physiological range and can be dynamically controlled and strictly monitored throughout the experiment to directly study the effects on the microvessels in the skeletal muscle being imaged.

These gas exchange chamber devices provide a unique and effective way to study the effects of tissue oxygen concentration on blood flow in the microcirculation that can be applied to different experimental models in combination with dynamically oscillating oxygen concentrations. The design of the gas exchange chamber enables it to be combined with other experimental methods with ease, allowing for instance, to study the simultaneous effects of multiple vasoactive stimuli on the blood flow in the microcirculation. Intravascular administration of different compounds, such as insulin and glucose, can be achieved in conjunction with variation of oxygen concentration in the tissue environment through the exchange chamber. More specifically, oxygen and insulin have both been shown to stimulate blood flow responses in the microcirculation, and these responses can be studied together by combining the gas exchange chamber with the hyperinsulinemia euglycemic clamp method, and the hemodynamic parameters can be measured using IVVM, as seen in the present thesis.

1.8 Summary

The microcirculation is a complex and dynamic system that is responsible for the delivery of nutrients and hormones, such as insulin, glucose, and oxygen, to myocytes, allowing the supply of blood to match the demand of muscle tissue throughout the body. Previous literature has demonstrated the intricate relationship between circulating insulin levels, glucose fixation in skeletal muscle, and blood flow regulation in response to differing oxygen levels. However, the interaction between insulin and oxygen in relation to the conversion of glucose into glycogen is yet to be thoroughly studied, despite the requirement of both substances to be present in order for glucose metabolism to occur. The combination of hyperinsulinemic euglycemic clamp, IVVM, and recently developed gas exchange chamber, enables us to address this gap in our knowledge. These methods allowed for direct visualization of skeletal muscle microcirculation while manipulating insulin, glucose, and oxygen concentrations simultaneously, hence gaining insights into the interactions of insulin and oxygen in muscle tissue as presented in Chapter 2.

References

Akerstrom, T., Goldman, D., Nilsson, F., Milkovich, S. L., Fraser, G. M., Brand, C. L., et al. (2019). Hyperinsulinemia does not cause de novo capillary recruitment in rat skeletal muscle. *Microcirculation*, 1985(104), 889. http://doi.org/10.1111/micc.12593

Alberts, B., Johnson, A., Lewis, J., et al. (2002). Molecular Biology of the Cell. 4th edition. New York: Garland Science; Blood Vessels and Endothelial Cells. Available from: https://www.ncbi.nlm.nih.gov/books/NBK26848/

Amiya, E., Watanabe, M. & Komuro, I. (2014). The Relationship between Vascular Function and the Autonomic Nervous System. *Ann Vasc Dis* **7**, 109–119. https://dx.doi.org/10.3400%2Favd.ra.14-00048

Augustin, H. G., & Koh, G. Y. (2017). Organotypic vasculature: From descriptive heterogeneity to functional pathophysiology. *Science (American Association for the Advancement of Science)*, 357(6353). https://doi.org/10.1126/science.aal2379

Bailey, J. K., Kindig, C. A., Behnke, B. J., Musch, T. I., Schmid-Schoenbein, G. W. & Poole, D. C. (2000). Spinotrapezius muscle microcirculatory function: effects of surgical exteriorization. *Am J Physiol Heart Circ Physiol*, 279, 3131-3137. https://doi.org/10.1152/ajpheart.2000.279.6.h3131

Balon, T. W., & Nadler, J. L. (1997). Evidence that nitric oxide increases glucose transport in skeletal muscle. *Journal of Applied Physiology*, 82(1), 359–363. http://doi.org/10.1152/jappl.1997.82.1.359

Baron, A. D., Steinberg,H., Brechtel, G. & Johnson, A. (1994). Skeletal muscle blood flow independently modulates insulin-mediated glucose uptake. *American Journal of Physiology - Endocrinology And Metabolism*, 266(2), 248-253. https://doi.org/10.1152/ajpendo.1994.266.2.e248

Bateman, R. M. (2003). Effect of inhibiting systemic nitric oxide overproduction on capillary morphology, hemodynamics and oxygen transport in skeletal muscle during sepsis. Available from ProQuest One Academic. Retrieved from https://www-proquest-com.qe2a-proxy.mun.ca/dissertations-theses/effect-inhibiting-systemic-nitric-oxide/docview/305238514/se-2?accountid=12378

Bauer, V. & Sotníková, R. (2010). Nitric oxide--the endothelium-derived relaxing factor and its role in endothelial functions. *General Physiology and Biophysics*, 29(4), 319-340. http://dx.doi.org/10.4149/gpb_2010_04_319

Bhattacharya, S., Dey, D. & Roy, S.S. (2007). Molecular mechanism of insulin resistance. *J. Biosci*. 32(2): 405–413. doi:10.1007/s12038-007-0038-8.

Bockman, E. L. (1983). Blood flow and oxygen consumption in active soleus and gracilis muscles in cats. American Journal of Physiology. *Heart and Circulatory Physiology*, 244(4), H546-H551. https://doi.org/10.1152/ajpheart.1983.244.4.h546

Bradley, E. A., Premilovac, D., Betik, A. C., Hu, D., Attrill, E., Richards, S. M., et al. (2019). Metformin improves vascular and metabolic insulin action in insulin-resistant muscle. *The Journal of Endocrinology*, 243(2), 85–96. doi: 10.1530/JOE-19-0067

Calbet, J. A., and Joyner, M. J. (2010). Disparity in regional and systemic circulatory capacities: do they affect the regulation of the circulation? *Acta Physiol*. 199, 393–406. doi: 10.1111/j.1748-1716.2010.02125.x

Cipolla, M. J. (2009). The Cerebral Circulation. San Rafael (CA): Morgan & Claypool Life Sciences; Chapter 2, Anatomy and Ultrastructure. Available from: https://www.ncbi.nlm.nih.gov/books/NBK53086/

Clerk, L. H., Vincent, M. A., Jahn, L. A., Liu, Z., Lindner, J. R. & Barrett, E. J. (2006). Obesity Blunts Insulin-Mediated Microvascular Recruitment in Human Forearm Muscle. *Diabetes*, 55(5), 1436-1442. doi: 10.2337/db05-1373.

Collins, D. M., Mccullough, W. T. & Ellsworth, M. L. (1998). Conducted vascular responses: communication across the capillary bed. *Microvasc. Res*, 56, 43–53. https://doi.org/10.1006/mvre.1998.2076

Davis, M. J., Hill, M. A., and Kuo, L. (2008). "Local regulation of microvascular perfusion," in Handbook of Physiology: Microcirculation, Second edition, eds R. F. Tuma, W. N. Duran, and K. Ley (San Diego, CA: Academic Press), 161–284. http://dx.doi.org/10.1002/cphy.cp020406

DeFronzo, R.A., Tobin, J.D. & Andres, R. (1979). Glucose clamp technique: a method for quantifying insulin secretion and resistance. *Am. J. Physiol. Metab*, 237(3): 214- 213. doi:10.1152/ajpendo.1979.237.3.

Dora, K. A. (2017). Conducted dilatation to ATP and K in rat skeletal muscle arterioles. *Acta Physiologica*, 219(1), 202-218. https://doi.org/10.1111/apha.12656

Duling, B. R. (1974). Oxygen sensitivity of vascular smooth muscle. II. In vivo studies. *Am J Physiol,* 227, 42–49. https://doi.org/10.1152/ajplegacy.1974.227.1.42

Duling, B. & Berne, R. (1970). Longitudinal Gradients in Periarteriolar Oxygen Tension: A Possible Mechanism for the Participation of Oxygen in Local Regulation of Blood Flow. *Circulation Research,* 27 (5), 669-678.

Ellis, C.G., Ellsworth, M.L. & Pittman, R.N. (1990). Determination of red blood cell oxygenation in vivo by dual video densitometric image analysis. *Am. J. Physiol,* 258(4): 1216-1223. doi:10.1152/ajpheart.1990.258.4.

Ellis, C.G., Ellsworth, M.L., Pittman, R.N. & Burgess, W.L. (1992). Application of image analysis for evaluation of red blood cell dynamics in capillaries. *Microvasc. Res,* 44(2): 214–225. doi:10.1016/0026-2862(92)90081-Y.

Ellsworth, M. L., Pittman, R.N. & Ellis, C.G. (1987). Measurement of hemoglobin oxygen saturation in capillaries. *Am. J. Physiol. Circ. Physiol*, 252(5): H1031–H1040. doi:10.1152/ajpheart.1987.252.5.H1031.

Ellsworth, M. L., Forrester, T., Ellis, C. G. & Dietrich, H. H. (1995). The erythrocyte as a regulator of vascular tone. *Am J Physiol,* 269, H2155-H2161. https://doi.org/10.1152/ajpheart.1995.269.6.h2155

Ellsworth, M. L, Ellis, C. G, & Sprague, R. S. (2016). Role of erythrocyte-released ATP in the regulation of microvascular oxygen supply in skeletal muscle. *Acta Physiologica*, 216(3), 265-276. https://doi.org/10.1111/apha.12596

Fraser, G. M. (2012). Modeling Oxygen Transport in Three-Dimensional Capillary Networks. Electronic Thesis and Dissertation Repository. 500. https://ir.lib.uwo.ca/etd/500

Fraser, G. M., Goldman, D. & Ellis, C. G. (2012a). Microvascular flow modelling using in vivo hemodynamic measurements in reconstructed 3D capillary networks. *Microciculation*, 19, 510-520. https://dx.doi.org/10.1111%2Fj.1549-8719.2012.00178.x

Fraser, G.M., Milkovich, S., Goldman, D., & Ellis, C.G. (2012b). Mapping 3-D functional capillary geometry in rat skeletal muscle in vivo. *American Journal of Physiology Heart and Circulatory Physiology*, 302(3):H654-664. https://doi.org/10.1152/ajpheart.01185.2010

Fu, Z., R. Gilbert, E. & Liu, D. (2012). Regulation of Insulin Synthesis and Secretion and Pancreatic Beta-Cell Dysfunction in Diabetes. *Curr. Diabetes Rev*, 9(1): 25–53. doi:10.2174/157339811309010025.

Furchgott R. F. (1988): Studies on relaxation of rabbit aorta by sodium nitrite the basis for the proposal that acid-activatible inhibitory factor from bovine retractor penis

is inorganic nitrite and the endothelium-derived relaxing factor is nitric oxide. In: Vasodilatation (Ed. P. M. Vanhoutte), pp. 401–412, Raven Press, New York.

Gutterman, D.D., Chabowski, D.S., Kadlec, A.O., Durand, M.J., Freed, J.K., Aissa, K.A. & Beyer, A.M. (2017). The Human Microcirculation: Regulation of Flow and Beyond. *Circ. Res*, 118(1): 157–172. doi:10.1161/CIRCRESAHA.115.305364.

Goldman, D., Fraser, G. M., Ellis, C. G., Sprague, R. S., Ellsworth, M. L. & Stephenson, A. H. (2012). Toward a multiscale description of microvascular flow regulation: O_2-dependent release of ATP from human erythrocytes and the distribution of ATP in a pillars networks. *Frontiers in Physiology*, 3, 1-11. doi: 10.3389/fphys.2012.00246

Hanson, M. S., Ellsworth, M. L., Achilleus, D., Stephenson, A. H., Bowles, E. A., Sridharan, M., Adder- ley, S. & Sprague, R. S. (2009). Insulin inhibits low oxygen-induced ATP release from human erythrocytes: implication for vascular control. *Microcirculation*, 16, 424–433. https://dx.doi.org/10.1080%2F10739680902855218

Hanson, M. S., Stephenson, A. H., Bowles, E. A. & Sprague, R. S. (2010). Insulin inhibits human erythrocyte cAMP accumulation and ATP release: role of phosphodiesterase 3 and phosphoinositide 3- kinase. *Exp. Biol. Med*, 235, 256–262. https://doi.org/10.1258/ebm.2009.009206

Hedman A, Berglund L, Esse´n-Gustavsson B, et al. (2000). Relationships between muscle morphology and insulin sensitivity are improved after adjustment for intra-individual variability in 70-year-old-men. *Acta Physiol Scand* 168:125-132. https://doi.org/10.1046/j.1365-201x.2000.00722.x

Higaki, Y., Hirshman, M. F., Fujii, N., & Goodyear, L. J. (2001). Nitric oxide increases glucose uptake through a mechanism that is distinct from the insulin and contraction pathways in rat skeletal muscle. *Diabetes*, 50(2), 241–247. http://doi.org/10.2337/diabetes.50.2.241

Hirai, D. M, Copp, S. W, Ferreira, L. F, Musch, T. I, & Poole, D. C. (2010). Nitric oxide bioavailability modulates the dynamics of microvascular oxygen exchange during recovery from contractions. *Acta Physiologica*, 200(2), 159-169. https://doi.org/10.1111/j.1748-1716.2010.02137.x

Ignarro L. J., Byrus R. E., Buga G. M., & Wood K. S. (1987). Endothelium-derived relaxing factor from pulmonary artery and vein possesses pharmacological and chemical properties identical to those of nitric oxide radical. *Circ. Res*. 61, 866–879. https://doi.org/10.1161/01.res.61.6.866

Jackson, W. F. (1987). Arteriolar oxygen reactivity: where is the sensor? *Am J Physiol*, 253, H1120–H1126. https://dx.doi.org/10.1113%2FJP270192

Jackson, W. F. (2016). Arteriolar oxygen reactivity: where is the sensor and what is the mechanism of action? *J. Physiol*, 594(18): 5055–5077. doi: 10.1113/JP270192.

Jackson, W. F. (2017). Boosting the signal: Endothelial inward rectifier K channels. *Microcirculation*, 24(3). https://doi.org/10.1111/micc.12319

James, D. E., Jenkins, A. B. & Kraegen, E. W. (1985). Heterogeneity of insulin action in individual muscles in vivo: eugylcemic clamp studies in rats. *American Journal of Physiology-Endocrinology and Metabolism*, 248(5), 567-574. doi: 10.1152/ajpendo.1985.248.5.E567

Jia, L., Bonaventura, C., Bonaven- tura, J. & Stamler, J. S. (1996). S-nitrosohaemoglobin: a dynamic activity of blood involved in vascular control. *Nature*, 380, 221–226. https://doi.org/10.1038/380221a0

Joyner, M. J., and Casey, D. P. (2014). Muscle blood flow, hypoxia and hypoperfusion. *J. Appl. Physiol*. 116, 852–857. doi: 10.1152/japplphysiol.00620.2013

Katayama, K., & Saito, M. (2019). Muscle sympathetic nerve activity during exercise. *J Physiol Sci*, 69, 589–598. https://doi.org/10.1007/s12576-019-00669-6

Kamga, C., Krishnamurthy, S. & Shiva, S. (2012). Myoglobin and mitochondria: A relationship bound by oxygen and nitric oxide. *Nitric Oxide*, 26(4), 251-258. https://doi-org.qe2a-proxy.mun.ca/10.1016/j.niox.2012.03.005

Kindig, C. A., Sexton, W. L., Fedde, M. R., & Poole, D. C. (1998). Skeletal muscle microcirculatory structure and hemodynamics in diabetes. *Respiration Physiology*, 111(2), 163-175. https://doi.org/10.1016/s0034-5687(97)00122-9

Kolka, C.M. & Bergman, R.N. (2010). Diabetic Complications. *Circ. Res*, 14(1): 13–19. doi:10.1007/s11154-012-9233-5.

Lillioja, S, Young, A. A, Culter, C. L, Ivy, J. L, Abbott, W. G. H, Zawadzki, J. K. & Bogardus, C. (1987). Skeletal muscle capillary density and fiber type are possible determinants of in vivo insulin resistance in man. *The Journal of Clinical Investigation*, 80(2), 415-424. https://doi.org/10.1172/jci113088

Lindbom L., Tuma, R. F. & Arfors, K. E. (1982). Blood flow in the rabbit tenuissimus muscle. Influence of preparative procedures for intravital microscopic observation. *Acta Physiol Scand*, 114, 121-127. https://doi.org/10.1111/j.1748-1716.1982.tb06960.x

Mahmoud, A. M., Szczurek, M. R., Blackburn, B. K., Mey, J. T., Chen, Z., Robinson, A. T., . . . Haus, J. M. (2016). Hyperinsulinemia augments endothelin-1 protein expression and impairs vasodilation of human skeletal muscle arterioles. *Physiological Reports*, 4(16), E12895-N/a. https://doi.org/10.14814/phy2.12895

McClatchey, P. M., Williams, I. M., Xu, Z., Mignemi, N. A., Hughey, C. C., McGuinness, O. P., et al. (2019). Perfusion controls muscle glucose uptake by altering the rate of glucose dispersion in vivo. *American Journal of Physiology-Endocrinology and Metabolism*, 317(6), 1022–1036. http://doi.org/10.1152/ajpendo.00260.2019

McClatchey, P. M., Williams, I. M., Xu, Z., Mignemi, N. A., Hughey, C. C., McGuinness, O. P., . . . Ellis, C. G. (2020). Reply to Letter to the Editor: Perfusion controls muscle glucose uptake by altering the rate of glucose dispersion in vivo. *American Journal of Physiology: Endocrinology and Metabolism*, 318(3), E313-E317. https://doi.org/10.1152/ajpendo.00508.2019

McCullough, W. T., Collins, D. M. & Ellsworth, M. L. (1997). Arteriolar responses to extracellular ATP in striated muscle. *Am. J. Physiol*, 272, H1886–H1891. https://doi.org/10.1152/ajpheart.1997.272.4.h1886

Mendelson, A. A., Milkovich, S., Hunter, T., Vijay, R., Choi, Y., Milkovich, S., . . . Ellis, C. G. (2021). The capillary fascicle in skeletal muscle: Structural and functional physiology of RBC distribution in capillary networks. *The Journal of Physiology*, 599(8), 2149-2168. https://doi.org/10.1113/jp281172

Palmer R. M. J., Ferrige A. G., Moncada S. (1987): Nitric oxide release accounts for the biological activity of edothe- lium-derived relaxing factor. Nature 327, 524–526; doi:10.1038/327524a0

Pittman, R. N. & Duling, B. R. (1973). Oxygen sensitivity of vascular smooth muscle. I. In vitro studies. *Microvasc Res*, 6, 202–211. https://doi.org/10.1016/0026-2862(73)90020-4

Popel, A.S. & Johnson, P.C. (2005). Microcirculation and Hemorheology. *Annu. Rev. Fluid. Mech*, 37: 43–69. doi:10.1146/annurev.fluid.37.042604.133933.

Prahl, S. (1999). Optical Absorption of Hemoglobin. https://omlc.org/spectra/hemoglobin/.

Ramos, P. A., Lytle, K. A., Delivanis, D., Nielsen, S., LeBrasseur, N. K., & Jensen, M. D. (2020). Insulin-Stimulated Muscle Glucose Uptake and Insulin Signaling in Lean and Obese Humans. *The Journal of Clinical Endocrinology and Metabolism*, 1-16. doi: 10.1210/clinem/dgaa919.

Remensnyder, J. P., Mitchell, J. H., and Sarnoff, S. J. (1962). Functional sympa- tholysis during muscular activity. Observations on influence of carotid sinus on oxygen uptake. *Circ. Res*. 11, 370–380. doi: 10.1161/01.RES.11.3.370

Richey, J. M. (2013). The vascular endothelium, a benign restrictive barrier? NO! role of nitric oxide in regulating insulin action. *Diabetes*, 62(12), 4006-4008. doi:http://dx.doi.org.qe2a-proxy.mun.ca/10.2337/db13-1395

Roy, T. K. & Secomb, T. W. (2014). Functional sympatholysis and sympathetic escape in a theoretical model for blood flow regulation. *Frontiers in Physiology*, 5, 192. https://doi.org/10.3389/fphys.2014.00192

Sandstrom, M. E., Zhang, S., Briton, J., Silva, J. P., Reid, M. B., Westerblad, H., & Katz, A. (2006). Role of reactive oxygen species in contraction-mediated glucose transport in mouse skeletal muscle. *Journal of Physiology,* 575, 251-262. doi: 10.1113/jphysiol.2006.110601

Segal, S. (2005). Regulation of Blood Flow in the Microcirculation. *Microcirculation.* 12, 33-45. http://doi.org/10.1080/10739680590895028

Sjoberg, K. A., Rattigan, S., Hiscock, N., Richter, E. A. & Kiens, B. (2011). A new method to study changes in microvascular blood volume in muscle and adipose tissue: real-time imaging in humans and rat. *Am J Physiol Heart Circ Physiol*, 301:H450-H458. https://doi.org/10.1152/ajpheart.01174.2010

Smith, A. F., Doyeux, V., Berg, M., Peyrounette, M., Haft-Javaherian, M., Larue, Anne-Edith, . . . Lorthois, Sylvie. (2019). Brain Capillary Networks Across Species: A few Simple Organizational Requirements Are Sufficient to Reproduce Both Structure and Function. *Frontiers in Physiology*, 10(233), 233. https://dx.doi.org/10.3389%2Ffphys.2019.00233

Sové, R. J., Milkovich, S., Nikolov, H., & Holdsworth, D. (2021). Localized oxygen exchange platform for intravital video microscopy investigations of microvascular oxygen regulation. *Frontiers in Physiology*, *12*, 505. https://doi.org/10.3389/fphys.2021.654928

Sprague, R.S., Bowles, E.A., Achilleus, D., Stephenson, A.H., Ellis, C.G. & Ellsworth, M.L. (2011). A selective phosphodiesterase 3 inhibitor rescues low PO2-induced ATP release from erythrocytes of humans with type 2 diabetes: implication for vascular control. *Am J Physiol* 301, H2466– H2472. https://doi.org/10.1152/ajpheart.00729.2011

Steinberg, H O, Brechtel, G, Johnson, A, Fineberg, N, & Baron, A D. (1994). Insulin-mediated skeletal muscle vasodilation is nitric oxide dependent. A novel action of insulin to increase nitric oxide release. *The Journal of Clinical Investigation*, 94(3), 1172-1179. https://dx.doi.org/10.1172%2FJCI117433

Tyml K., & Budreau, C.H. (1991). A new preparation of rat extensor digitorum longus muscle for intravital investigation of the microcirculation. *International Journal of Microcirculation, Clinical and Experimental,* 10(4):335-343.

Wang, H., Wang, A. X., Aylor, K., & Barrett, E. J. (2013). Nitric Oxide Directly Promotes Vascular Endothelial Insulin Transport. *Diabetes*, 62(12), 4030-4042. https://doi.org/10.2337/db13-0627

Williams, I. M., Valenzuela, F. A., Kahl, S. D., Ramkrishna, D., Mezo, A. R., Young, J. D., et al. (2018). Insulin exits skeletal muscle capillaries by fluid-phase transport. *The Journal of Clinical Investigation*, 128(2), 699–714. http://doi.org/10.1172/JCI94053

Wilson, D. F., & Matschinsky, F. M. (2019). Oxygen dependence of glucose sensing: role in glucose homeostasis and related pathology. *Journal of Applied Physiology*, 126(6), 1746–1755. http://doi.org/10.1152/japplphysiol.00047.2019

Wray, D. W., Witman, M. A. H., Ives, S. J., McDaniel, J., Fjeldstad, A. S., Trinity, J. D., Richardson, R. S. (2011). Progressive handgrip exercise: Evidence of nitric oxide-dependent vasodilation and blood flow regulation in humans. *American Journal of Physiology,* 300(3), H1101-H1107. https://doi.org/10.1152/ajpheart.01115.2010

Chapter 2: Clamping skeletal muscle PO_2 eliminates hyperinsulinemic microvascular blood flow response

(In preparation for submission to *Microcirculation*)

2.1 Introduction

The microcirculation plays a crucial role in the regulation of muscle tissue metabolism and is impacted by a variety of vasoactive stimuli. Endogenous vasoactive agents include oxygen concentration, carbon dioxide, and humoral substances such as adenosine and insulin. Insulin, a peptide hormone released from cells within the pancreas, has been shown to increase blood flow in skeletal muscle vasculature, as well as act as an important regulator of blood glucose levels (Baron et al., 1994; Akerstrom et al., 2019; Zierath & Krook, 2000). It is well established that insulin promotes the translocation of the GLUT4 receptor to the cell surface, increasing glucose uptake into skeletal muscle myocytes (Zierath & Krook, 2000). Skeletal muscle is therefore a critical tissue for the disposal of blood glucose and serves as the primary storage pool of glycogen within the body (Zierath & Krook, 2000). Previous studies have suggested that insulin itself causes vasodilation through stimulating the release of nitric oxide (NO) from the endothelial cells, which dilate arterioles to cause an increase in blood flow to downstream vascular beds (Steinberg et al., 1994). Increasing flow to the microcirculation increases the delivery of glucose to the skeletal muscle, and therefore allows for an increase of glucose uptake into the muscle (Baron et al., 1994; McClatchey et al., 2019). Enhanced glucose uptake has been shown to occur with increases in NO independently of insulin levels, due to the effect that NO has on vascular tone (Hiagki et al., 2001; Balon & Nadler. 1997).

Whether or not insulin directly interacts with other known vasoactive mechanisms remains to be elucidated.

In addition to insulin and glucose, oxygen is an essential material for oxidative metabolism that is delivered to skeletal muscle through the capillaries. It has been shown that changes in blood flow occur in the microcirculation in response to changing metabolic demand of the muscle tissue, often seen in exercise states (Ghonaim et al., 2011; Jackson et al., 2010). Blood flow to the microcirculation will increase to deliver more oxygen in response to hypoxia or elevated oxidative metabolism, for example during exercise (Segal, 2005; Jackson et al., 2010; Hudlicka, 1985). While there is currently little evidence in the literature connecting oxygen concentrations with insulin-mediated glucose uptake, recently it has been suggested that the sensing, and therefore the uptake of glucose is dependent on oxygen concentrations within the muscle (Wilson & Matchinsky, 2019). It was demonstrated experimentally that sufficient levels of oxygen must be present for pancreatic cells to sense, and subsequently uptake available glucose in order for glucose metabolism and oxidative phosphorylation to occur, and computational modelling suggests similar tendencies in muscle tissue as well (Wilson & Matchinsky, 2019). Additionally, reactive oxygen species (ROS), which are by-products of oxidative metabolism, have also been studied as a potential regulator of muscle glucose uptake. One study found that ROS, particularly H_2O_2, play an important role in contraction-mediated activation of glucose transport in fast-twitch muscle (Sandstrom et al., 2006). This suggests a potential link between insulin-mediated glucose uptake and oxygen concentrations in the microcirculation; New methods have been developed to directly study the blood flow responses in the microvasculature to these stimuli.

Intravital video microscopy (IVVM) has been an effective method of studying the capillaries in skeletal muscle preparations, and emerging technologies have allowed for the measurements of the rate of blood flow through the microcirculation (Japee et al., 2004). Other methods utilizing the IVVM apparatus have also been developed that allow for the quantification of the oxygen saturation of red blood cells passing through capillaries (Ellis et al., 1990). These methodologies are particularly important in measuring the changes in blood flow and oxygen saturation in the capillaries due to the effects of different factors, such as changing insulin levels or imposing local oxygen concentration perturbations, either separately or together. By combining IVVM, hyperinsulinemic euglycemic clamp, and direct oxygen perturbations, the interacting effects these compounds have on blood flow in the microcirculation can be studied directly.

Given the impact that both oxygen and insulin have on microvascular blood flow, the ability to increase flow and therefore promote glucose uptake, it is reasonable to consider a potential interaction between these vasoactive stimuli. In the present study we aimed to address the hypothesis that blood flow responses to insulin are partially mediated by local metabolic demand reflecting increased oxygen consumption required to fix glucose. To address this hypothesis, we quantified the in vivo hyperinsulinemic blood flow response in skeletal muscle capillaries in an isolated preparation where all oxygen was supplied by the endogenous microvasculature. In order to test the oxygen dependence of the hyperinsulinemic response, we repeated this quantification while the muscle was interfaced with a microfluidic gas exchange chamber to clamp tissue gas concentrations. Our data shows that fixing gas concentrations within the muscle

eliminates the expected insulin mediated flow response, and that microvascular perfusion dynamically matches tissue oxygen conditions imposed by the exchange chamber irrespective of the hyperinsulinemic state.

2.2 Materials and Methods

2.2.1 Animal Surgery

16 male Sprague Dawley rats (161g - 204g) were used in the described experiments. Rats were obtained from Charles River Laboratories and were housed in Animal Care facilities in the Health Sciences Centre and were allowed to acclimatize for one week. Rats were fed Teklad 2018 (Envigo, Indianapolis, IND, USA) standard rodent chow. All animal protocols were approved by Memorial University Animal Care Committee.

On the day of testing, animals were anesthetized with a 65 mg/kg intraperitoneal injection of sodium pentobarbital (Euthanyl, Bimeda, Cambridge, ON, Canada). Following induction, depth of anaesthesia was assessed with palpebral reflex and toe pinch prior to the start of surgery to verify the animal was sufficiently anesthetized. Once in the surgical plane, a rectal temperature probe was inserted to monitor the body temperature of the animal throughout the experiment. Physiological temperatures were maintained between 36 - 37°C using a heated mat and/or a heat lamp as necessary.

To facilitate surgical instrumentation, an incision was made between the clavicle and jaw along the midline, as described previously (Fraser et al., 2012). The left common carotid artery was blunt dissected and isolated, allowing it to be cannulated with 0.58mm

outside diameter polyethylene tubing (Intramedic, BD, Franklin Lakes, NJ, USA). The carotid cannula was perfused with heparinized saline connected to a pressure infusion bag (C-Fusor, Smith-Medical, Minneapolis, MN, USA) and a momentary valve integrated into a blood pressure transducer to maintain patency throughout the experiment. The carotid cannula was connected to a pressure transducer (TruWave 3, Edwards Lifesciences, Irvine, CA, USA) that allowed for continuous monitoring and recording of mean arterial blood pressure and heart rate. Digital output from the blood pressure analyzer (400a, Digi-Med, Louisville, KY, USA) was recorded using the manufacturer's software and saved to text file. Custom double cannulas were fabricated to join 2 lengths of 0.635 mm internal diameter Silastic tubing (Dow Corning, Midland, MI, USA) into a single cannula for insertion into the jugular vein (Figure 2.1). The right external jugular vein was blunt dissected, isolated, and cannulated with the double cannula. One length of the double cannula was connected to an infusion pump (PhD 2000, Harvard Apparatus, Holliston, MA, USA) to deliver heparinized saline (1 U/ml, 0.5 ml/kg/hour) for fluid resuscitation, and the other length was tied off, and later connected to infusion pumps for insulin and glucose for the hyperinsulinemic euglycemic clamp. Maintenance anesthetic (32.8 mg/kg) was administered via the jugular cannula every 30 minutes or as needed. Depth of anesthesia was frequently evaluated by assessing the animal's response to nociceptive stimuli, and by monitoring heart rate variability and mean arterial blood pressure. A tracheotomy was performed to allow mechanical ventilation with an FiO_2 of 30 - 35% O_2 with the balance of N_2. Initial ventilation rate and volume was determined based on animal weight as per the manufacturer's instructions. Following the tracheotomy, the neck incision was sutured closed using a continuous lock stitch.

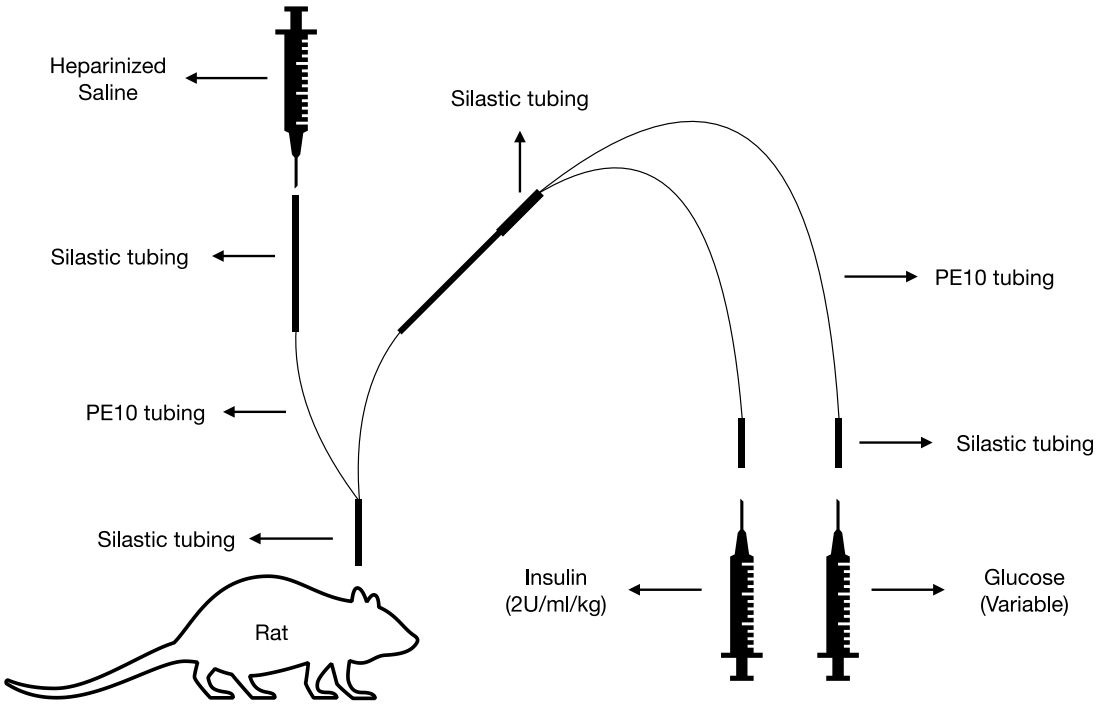

Figure 2.1 Apparatus for glucose and insulin infusion into the jugular vein during hyperinsulinemic euglycemic clamp. The components of the custom double cannulas are shown, which are inserted into the right jugular vein of the rat for administration of insulin, glucose, and saline for fluid resuscitation. Insulin and glucose are placed in infusion pumps for continuous infusion throughout the hyperinsulinemic euglycemic clamp. Heparinized saline is connected via a t-connector (not shown) that allows for administration of additional anesthetic as needed.

Following the neck surgery, a small section of skin was removed from the right lower hindlimb and the overlying connective tissue was blunt dissected to expose and isolate the extensor digitorum longus (EDL), as described previously (Fraser et al., 2012; Tyml & Budreau, 1991). A silk ligature was tied to the isolated distal tendon of the EDL before cutting the tendon to free the muscle from its insertion. The EDL muscle was reflected over the objective on the stage of an inverted microscope (Olympus IX73, Tokyo, Japan). The EDL was fixed at approximately in situ length using the ligature attached to the tendon, covered with a polyvinylidene chloride film (Saran, Dow Corning, MI, USA), bathed in warm saline, and gently compressed with a glass coverslip and microscope slide secured to the stage with a thin bead of vacuum grease on two sides (Dow Corning, Midland, MI, USA). The animal was allowed to acclimatize on the stage for 30 minutes following completion of the EDL setup. Following this acclimatization, and when the animal reached a body temperature of 36 °C and MAP was above 80 mmHg, an arterial blood sample was collected and loaded onto a CD4+ blood gas analyzer cartridge and inserted into a VetScan iSTAT (Abbott Point of Care Inc., Princeton, NJ, USA). Partial pressure of carbon dioxide (PCO_2) and partial pressure of oxygen (PO_2) were maintained at physiological levels by adjusting ventilation rate and volume as needed.

2.2.2 Intravital Microscopy Setup

The microscopy imaging setup was composed of an inverted microscope (Olympus IX73, Tokyo, Japan) fitted for transillumination with a 300W xenon light

source (Sutter Lambda LS, San Francisco, CA, USA). A parfocal beam splitter (OptoSplit II bypass, Cairn, Kent, UK), fitted with a 80:20, reflection:transmission mirror, connected to the side observation port of the microscope with the reflected light path passing through a 420 nm bandpass filter (isosbestic wavelength) and the transmitted beam passing through a 438 nm (oxygen-sensitive) filter; this allowed for simultaneous and parfocal capture of video sequences at both wavelengths using a single camera. Video recordings were made using an Orca Flash4.0 v3 scientific digital camera (Hamamatsu, Tokyo, Japan) connected to a desktop computer. HCImage Live software (Hamamatsu, Tokyo, Japan) was used to display and capture microscopic images.

2.2.3. Experiment 1a

At baseline conditions, an extended depth of field (EDF) map across the surface of the EDL muscle was recorded. Manual EDF recordings begin at the surface of the muscle and progressively focusing into the muscle to a depth of approximately 100 μm over 1 minute. The resulting video sequence is processed to produce functional images, analogous to a mean intensity projection images, that show the 2D geometry of flowing microvessels within the observed volume. In addition to the map, EDF recordings were captured at four different fields of view within the EDL. Following the EDF recordings, 1 minute intravital videos of the microcirculation were recorded at multiple focal planes within the four fields of view. Focal planes with the highest number of in focus capillaries were selected for video capture. All video recordings were captured using a 10X objective at 30 frames/second.

After the completion of the baseline recordings, a hyperinsulinemic euglycemic clamp procedure was performed by simultaneously infusing glucose (50%) and insulin (HumulinR, 2 U/ml/kg/hr) diluted with heparinized saline, using the double cannula inserted in the jugular vein. A glucometer (CONTOUR NEXT ONE, Ascensia Diabetes Care, Mississauga, ON, Canada) was used to measure blood glucose concentration using blood samples taken from a small cut at the tip of the tail. Glucose infusion rates were titrated to achieve normoglycemic levels, while insulin was infused at a constant rate. Euglycemia was defined as three consecutive stable blood glucose measurements between 5 – 7 mM (Leonard et al., 2005). Once euglycemia was achieved, recordings of microvascular blood flow were repeated in the same fields of view that were captured at baseline as described above. At the end of data collection, the animal was euthanized with an intravenous injection of sodium pentobarbital (150 mg/kg) (Figure 2.2).

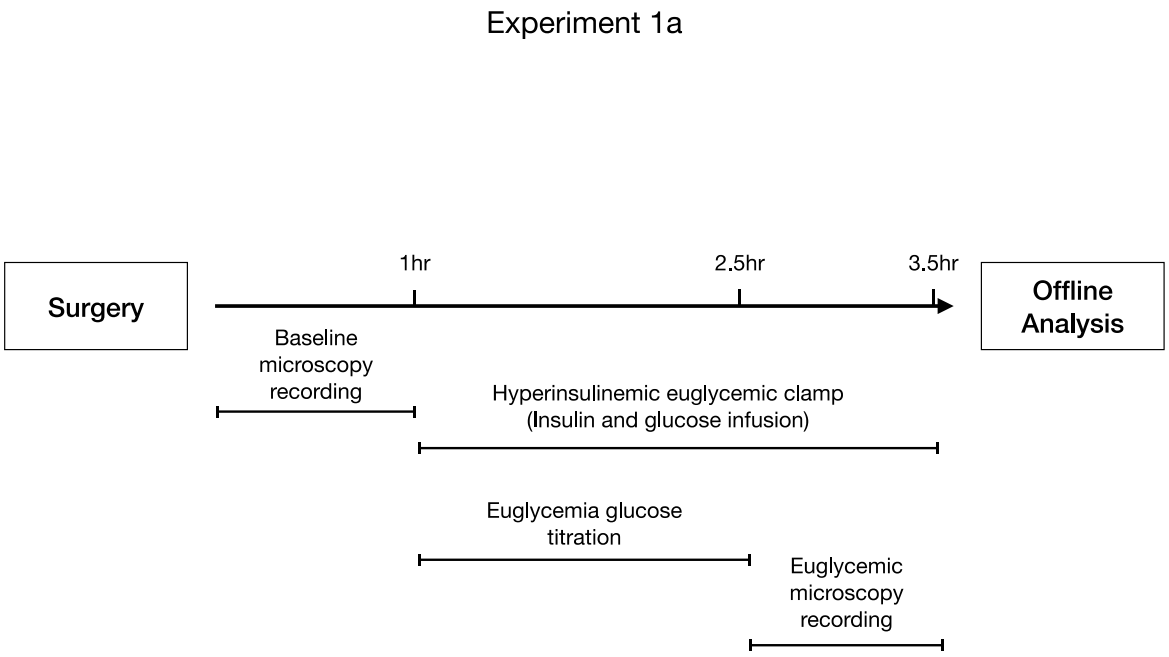

Figure 2.2 Timeline of the experimental protocol for Experiment 1a. Following the surgery to prepare the animal for intravital video microscopy (IVVM) imaging, baseline recordings of the extensor digitorum longus (EDL) muscle microcirculation are captured. Upon completion of the baseline recordings, the hyperinsulinemic euglycemic clamp begins. Insulin is infused at a steady rate, while glucose is infused at varying rates until a steady state of normal blood glucose levels, i.e. euglycemia, is achieved. Once this occurs, recordings that were captured at baseline are then repeated.

2.2.4. Experiment 1b

The same protocols were followed during baseline captures as described above for Experiment 1a with the following additions. To ensure the effects on the microvascular blood flow following the hyperinsulinemic euglycemic clamp were due to the introduction of high insulin and glucose infusions, and not an effect of time or fluid delivery during the clamp, a sham clamp was performed on a separate group of animals. Using the double cannula, two separate infusions of heparinized saline were delivered into the jugular vein to match infusion rates of insulin, and time matched average rate of glucose infusion used during Experiment 1a. Sham insulin infusion consisted of 1 ml/kg/hr of heparinized saline to match the volume of insulin infused in experiment 1a. Sham glucose infusion rates of heparinized saline were determined based on the average glucose infusion rates over time and normalized to body weight, and the duration of the sham glucose infusion matched the average time to reach euglycemia from experiment 1a. Blood glucose measurements were conducted as described above. After the target time for the sham euglycemic clamp was reached recordings captured at baseline were repeated (Figure 2.3), following which the animal was euthanized.

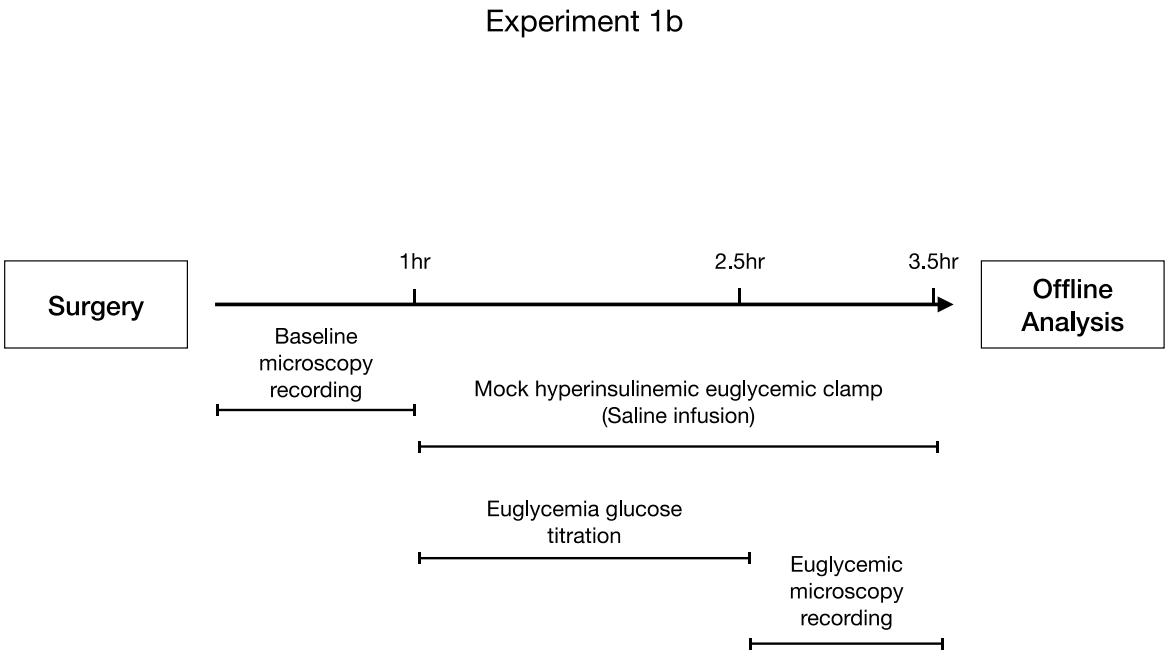

Figure 2.3 Timeline of the experimental protocol for Experiment 1b. Following the surgery to prepare the animal for intravital video microscopy (IVVM) imaging, baseline recordings of the extensor digitorum longus (EDL) muscle microcirculation are captured. Upon completion of the baseline recordings, the sham hyperinsulinemic euglycemic clamp is started, which consists of infusing saline at similar rates as insulin and glucose in the real clamp procedures. Saline was continuously infused for the average period of time it took to reach euglycemia in Experiment 1a. Once this was complete, recordings that were captured at baseline are then repeated.

2.2.5. Experiment 2

At baseline conditions, an EDF map was collected as described above to visualize the connectivity of the microvasculature in the EDL muscle. To evaluate oxygen dependence of blood flow, four-minute recordings were taken in four different fields of view across the muscle at a focal depth within 50 μm of the surface, while attempting to maximize the number of in focus capillaries. Oxygen concentration at the surface of the muscle was oscillated from 7%-12%-2%-7% for one minute each during the four-minute recordings in each field using a gas exchange chamber as described below (Sové et al., 2021). CO_2 was kept stable at 5%, with N_2 making up the balance of the gas mixture. Gases were delivered to the surface of the EDL muscle using a three-dimensionally (3D) printed gas exchange chamber as described previously (Sové et al., 2021). Briefly, the gas exchange chamber consisted of a 3D printed base designed to fit in the stage insert of the microscope, with a micro gas channel formed between a 45 x 55 mm glass coverslip, 3D printed gas channel gasket, and an overlying 3D printed layer to mount the exchange membrane and connections for the gas supply. This device contains an exchange window (5 x 3.5mm) covered with a 100 μm oxygen permeable membrane fabricated by spin coating poly(dimethyl siloxane) (PDMS) onto a standard glass slide. PDMS membranes were removed from the glass slide and cut into 30 x 30 mm sheets before being mounted to the gas exchange chamber. The assembled device was connected by plastic tubing to a triple-inlet manifold supplied by three computer-controlled mass flow meters (SmartTrak100, Sierra Instruments, Monterey, CA, USA) for each gas channel, with a frequency response of <300 ms. The EDL muscle was placed over the exchange window of the device and isolated from room air as described above. In this configuration, the

muscle surface viewable by the microscope is interfaced with the gas channel via the gas permeable PDMS membrane allowing for rapid changes in tissue oxygen concentrations to be imposed similar to what has been described previously (Figure 2.4) (Sové et al., 2021). Gas concentrations from the mass flow meters were dynamically controlled by custom MATLAB software allowing changes in oxygen concentration to be triggered automatically at the appropriate time and sequence.

A hyperinsulinemic euglycemic clamp was performed as described in Experiment 1a after baseline captures were completed. After euglycemia was achieved, the fields of view captured at baseline were recorded again, imposing the same oxygen oscillation. Upon completion of these recordings, the animal was euthanized (Figure 2.5).

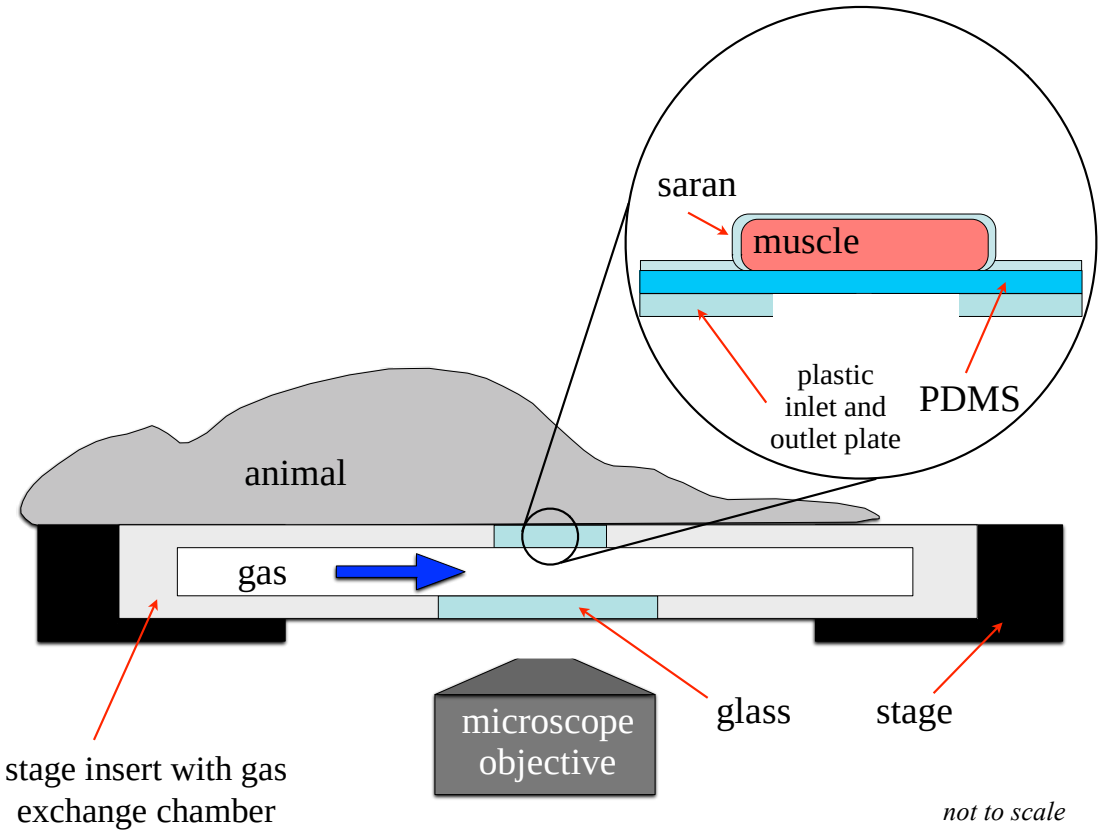

Figure 2.4 Adapted experimental setup of the animal placed atop the gas exchange chamber inserted into the microscope stage. The chamber fitted into the inverted microscope stage, with the muscle aligned over the PDMS membrane and covered with a small piece of gas impermeable polyvinylidene film (Saran, Dow Corning, Midland, MI, USA), therefore the muscle is affected only by the gases flowing through the chamber (Adapted from Sové et al., 2021, used under Creative Commons License).

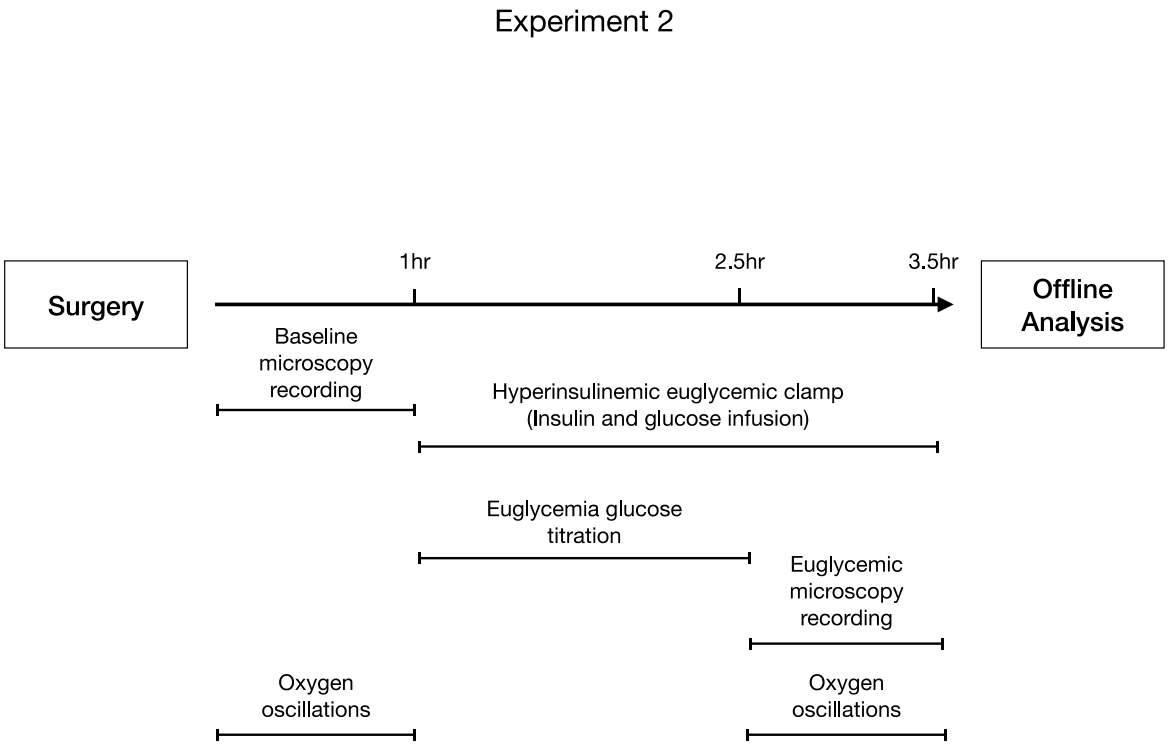

Figure 2.5 Timeline of the experimental protocol for Experiment 2. Following the surgery to prepare the animal for intravital video microscopy (IVVM) imaging, baseline recordings of the extensor digitorum longus (EDL) muscle microcirculation are captured while performing oxygen oscillations using the gas exchange device. Upon completion of the baseline recordings, the hyperinsulinemic euglycemic clamp begins. Insulin is infused at a steady rate, while glucose is infused at varying rates until a steady state of normal blood glucose levels, or euglycemia, is achieved. Once this occurs, recordings that were captured at baseline are then repeated in the hyperemic muscle while performing the same oxygen oscillations as before.

2.2.6. Offline Analysis and Statistics

Offline analysis was conducted using custom software written in MATLAB (Mathworks, Natick, Mass, MA, USA). The software generated MP4 videos of captured sequences and functional images including variance and sum of absolute difference (SAD) images used to facilitate identification of in focus vessel segments for analysis. In focus capillaries with single file RBC flow were semi-automatically selected for analysis and space time images (STIs) were generated at each wavelength as described previously. STIs were analyzed using the custom software package and frame-by-frame measurements for velocity, lineal density, RBC supply rate, and oxygen saturation were written out to text files for aggregation and statistical analysis (Ellis et al., 1992). All reported values represent per-animal mean hemodynamic measurements with standard deviation taken from analyzed capillaries at baseline and euglycemia for the experiment protocols unless otherwise noted. For experiment 2, mean values were calculated from measurements taken from the last 15s of the 7%-12%-2%-7% steps of the oscillation. For the first step of the oscillation, measurements from the entire minute were included in the mean values to include periodic variability in blood flow. EDF maps were generated for reference using custom mapping software written in MATLAB as described previously (Fraser et al., 2012).

Statistical analysis of the hemodynamic data was completed using Prism software (Graphpad, CA, USA). Paired t-tests were used for comparisons of hemodynamic measurements between baseline and euglycemic conditions paired for each animal. Unpaired t-tests were used for the comparison of glucose infusion rate (GIR) between experiment 1 and 2. Analysis of Variance (ANOVA) multiple comparison tests with

Tukey post-hoc tests were used to compare systemic animal data between all three experiments and hemodynamic data at each oxygen concentration for both conditions in Experiment 2. A p value of < 0.05 was considered significant.

2.3 Results

2.3.1. Systemic Physiological and Clamp Measurements

Systemic physiological parameters for each animal group are shown in Table 2.1; Similarly, blood gases were sampled during experiments were similar for each group and condition shown in Table 2.2. Blood glucose levels were not significantly different during baseline or hyperinsulinemic euglycemic conditions between experiments as per experimental design, and glucose infusion rates during hyperinsulinemic euglycemic clamp also did not vary significantly between experiments (Figure 2.6).

Table 2.1 Mean and standard deviation of systemic animal data for each experiment protocol.

	Experiment 1a (N = 6)	**Experiment 1b (N = 4)**	**Experiment 2 (N = 6)**
Animal weight (g)	179.2 ± 11.3	184.8 ± 16.5	189.8 ± 9.3
Mean arterial pressure (mmHg)	95.7 ± 6.0	98.4 ± 6.0	91.3 ± 3.6
Systolic blood pressure (mmHg)	100.0 ± 5.8	103.4 ± 5.7	96.3 ± 3.6
Diastolic blood pressure (mmHg)	89.3 ± 6.2	90.9 ± 6.7	84.2 ± 4.0
Heart rate (beats/min)	406.7 ± 24.5	415.2 ± 25.3	397.9 ± 10.1
Respiratory rate (breaths/min)	83.3 ± 1.2	82.8 ± 2.4	83.0 ± 1.1
Respiratory volume (cc)	1.2 ± 0.1	1.2 ± 0.1	1.3 ± 0.1

Note: Blood pressure measurements were missing from one animal in Experiment 2.

Table 2.2 Mean and standard deviation of data collected from arterial blood gas samples for each experiment.

	Experiment 1a (N = 6)	**Experiment 1b (N = 4)**	**Experiment 2 (N = 6)**
pH	7.4 ± 0.03	7.4 ± 0.03	7.4 ± 0.03
PCO_2 (mmHg)	50.4 ± 5.3	48.1 ± 3.1	50.1 ± 5.6
PO_2 (mmHg)	130.9 ± 21.2	104.7 ± 28.1	130.8 ± 16.2
BEecf (mmol/L)	4.6 ± 2.3	5.0 ± 1.7	5.3 ± 1.8
HCO_3 (mmol/L)	29.7 ± 2.1	29.9 ± 1.5	30.2 ± 1.9
TCO_2 (mmol/L0	31.0 ± 2.3	31.3 ± 1.6	31.7 ± 2.2
SO_2 (%)	98.6 ± 0.8	96.6 ± 3.4	98.7 ± 0.5
Lac (mmol/L)	1.1 ± 0.4	0.9 ± 0.4	1.1 ± 0.5

Note: PCO_2: partial pressure of carbon dioxide; PO_2: partial pressure of oxygen; BEecf: base excess in the extracellular fluid compartment concentration; HCO_3: bicarbonate concentration; TCO_2: total carbon dioxide; SO_2: oxygen saturation; Lac: lactate concentration

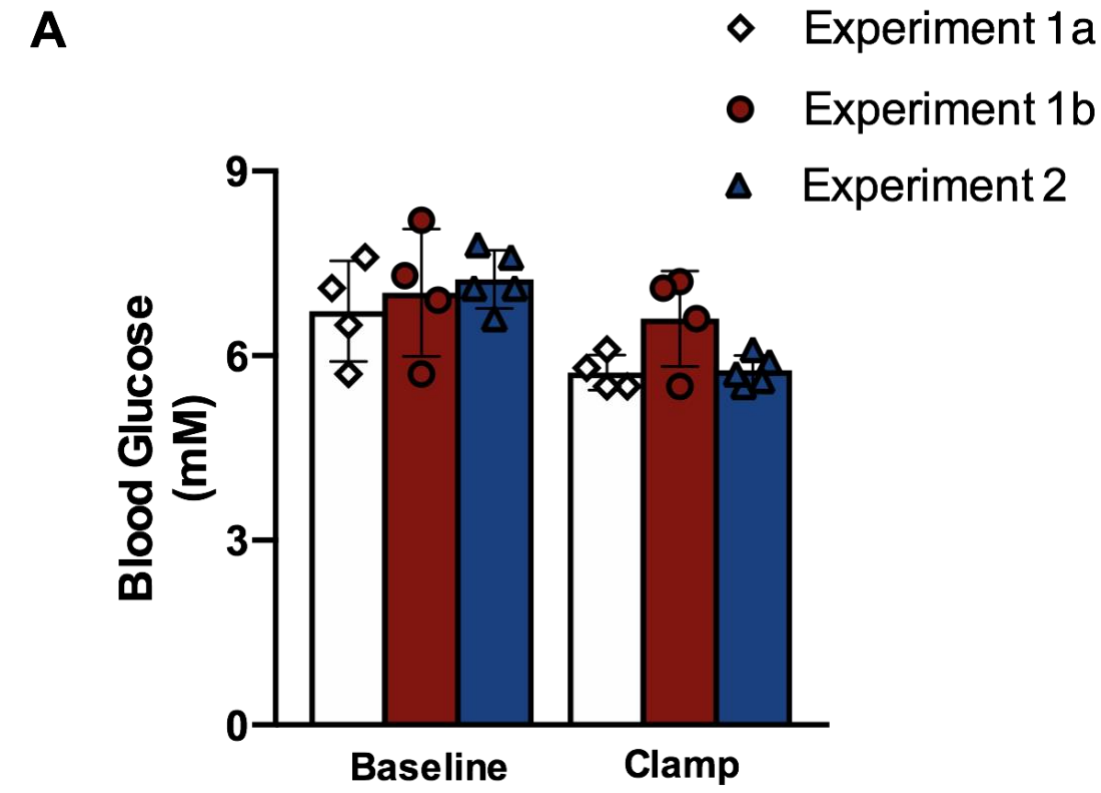
A
Experiment 1a
Experiment 1b
Experiment 2
Blood Glucose (mM)
9
6
3
0
Baseline
Clamp

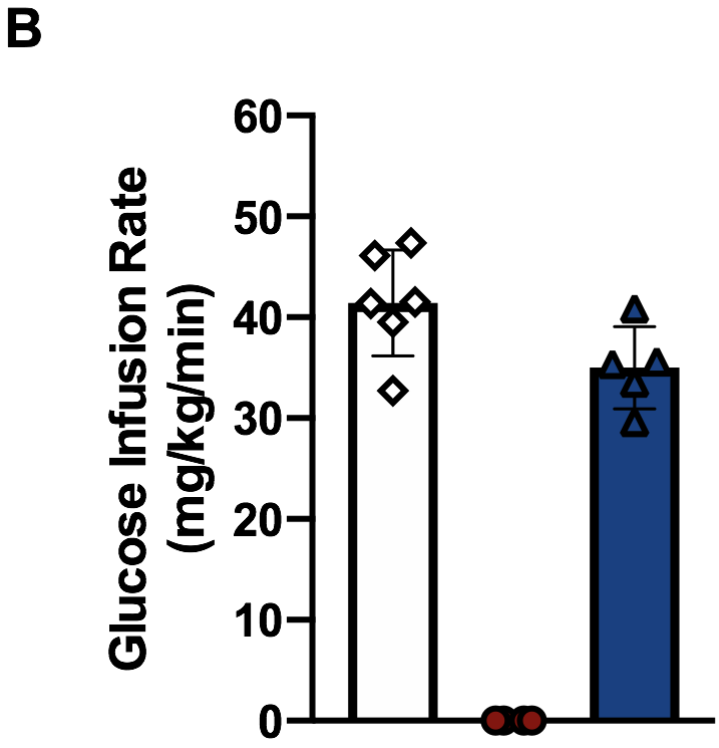
B
Glucose Infusion Rate (mg/kg/min)
60
50
40
30
20
10
0

Figure 2.6 Blood glucose measurements during baseline and hyperinsulinemic euglycemic clamp for each experimental protocol. Experiment 1a and 1b were conducted using a glass microscope stage insert and Experiment 2 used a gas exchange stage insert. A) Mean blood glucose level at baseline and hyperinsulinemia euglycemic clamp conditions. Mean values were calculated during capturing periods for all experiment protocols and blood glucose was measured from tail blood samples using a standard glucose meter. Euglycemia was achieved when a stable blood glucose level between 5 - 7 mM was reached. B) Mean glucose infusion rate during hyperinsulinemic euglycemic clamp conditions for experiment 1a and 1b. Glucose infusion rates were adjusted during euglycemic clamp to achieve normoglycemic blood levels and to ensure the values were maintained in this range. Each point represents a per animal mean, with error bars showing standard error of the mean. N = 6 for experiment 1a, 2 for experiment 1b, and 5 for experiment 2.

2.3.2. Results: Experiment 1a and 1b

For Experiment 1a hemodynamic parameters, a total of 677 capillaries were analyzed at baseline conditions and 552 capillaries were analyzed at euglycemic conditions across 6 animals. For Experiment 1b, 501 capillaries were analyzed at baseline and 417 capillaries were analyzed at euglycemic conditions across 4 animals. Mean RBC velocity for Experiment 1a was found to be different at baseline (186.1 ± 54.8 μm/sec) and euglycemic clamp (259.7 ± 59.3 μm/sec) ($p = 0.02$). For Experiment 1b, mean RBC velocity was 219.6 ± 48.6 μm/sec at baseline and 230.3 ± 70.8 μm/sec following sham euglycemic clamp (Figure 2.7). Mean RBC supply rate for Experiment 1a was also found to be different at baseline (8.9 ± 3.1 cells/s) and euglycemic clamp (14.2 ± 4.9 cells/sec) ($p = 0.01$). For Experiment 1b, mean RBC supply rate was 11.1 ± 1.9 cells/sec at baseline and 12.1 ± 4.2 cells/sec at sham clamp (Figure 2.8). Mean hematocrit for Experiment 1a was 17.3 ± 0.6% at baseline and 17.6 ± 2.2% at euglycemic clamp. For Experiment 1b, mean hematocrit was 18.7 ± 1.7% at baseline and 17.7 ± 1.9% at sham clamp (Figure 2.9).

For saturation measurements, 659 capillaries were analyzed at baseline conditions and 528 capillaries were analyzed at euglycemia across 6 animals in Experiment 1a. In Experiment 1b, 464 capillaries were analyzed at baseline and 397 capillaries were analyzed at euglycemic conditions across 4 animals. The mean RBC oxygen saturation (SO_2) for Experiment 1a was 42.8 ± 4.6% at baseline and 48.0 ± 7.6% at euglycemic clamp. Mean SO_2 for Experiment 1b was 48.3 ± 5.2% at baseline and 49.0 ± 10.1% following sham clamp (Figure 2.10). There were no significant differences in any of the

hemodynamic or SO_2 measurements between baseline and sham euglycemic conditions in Experiment 1b.

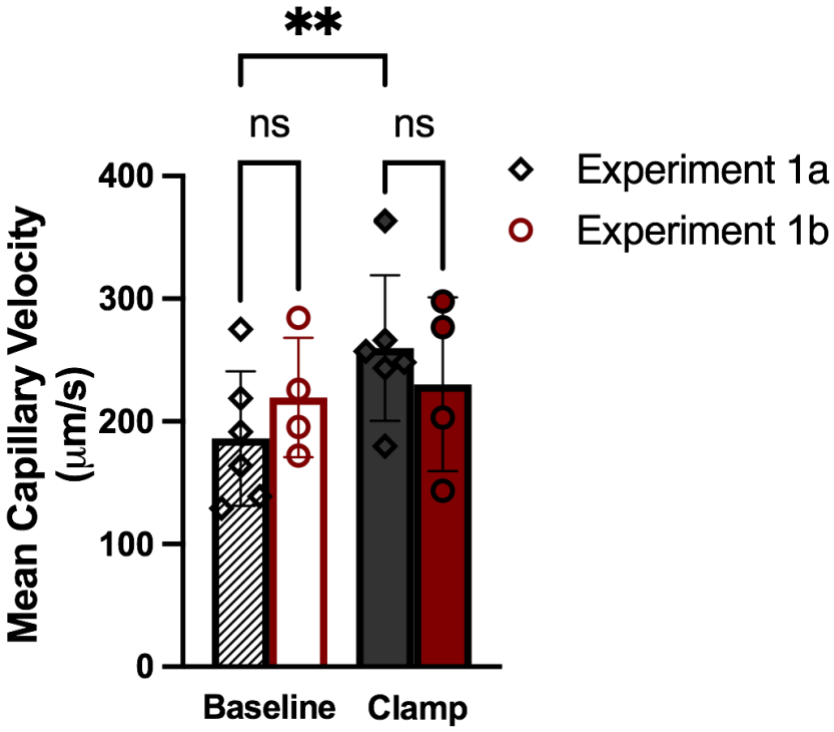

Figure 2.7 Mean capillary red blood cell velocity measured during baseline and euglycemic clamp. Measurements of red blood cell velocity were taken in the extensor digitorum longus muscle, with Experiment 1a consisting of baseline and hyperinsulinemic euglycemic conditions and Experiment 1b consisting of baseline and sham clamp conditions (using saline). Each data point represents a per animal mean and error bars showing standard error of the mean. For 1a, velocity increased from 186 μm/sec at baseline to 260 μm/sec at hyperinsulinemic euglycemia ($p = 0.02$). N = 6 animals (677 capillaries at baseline, and 552 capillaries at clamp). For 1b, velocity was 220 μm/sec at baseline and 230 μm/sec following saline infusion. N = 4 animals (501 capillaries at baseline, and 417 capillaries at clamp). **: $p < 0.05$, compared to baseline (Paired t-test).

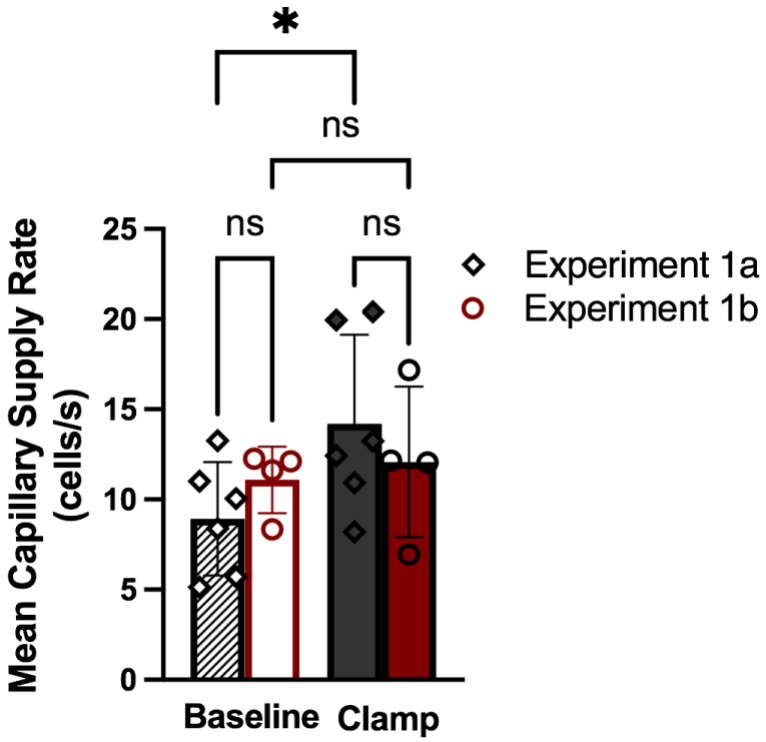

Figure 2.8 Mean capillary red blood cell supply rate measured during baseline and euglycemic clamp. Measurements of red blood cell supply rate were taken in the extensor digitorum longus muscle, with Experiment 1a consisting of baseline and hyperinsulinemic euglycemic conditions and Experiment 1b consisting of baseline and sham clamp conditions (using saline). Each data point represents a per animal mean and error bars showing standard error of the mean. For 1a, supply rate increased from 9 cells/sec at baseline to 14 cells/sec at hyperinsulinemic euglycemia ($p = 0.01$). N = 6 animals (677 capillaries at baseline, and 552 capillaries at clamp). For 1b, supply rate was 11 cells/sec at baseline and 12 cells/sec following saline infusion. N = 4 animals (501 capillaries at baseline, and 417 capillaries at clamp). *: $p < 0.05$, compared to baseline (Paired t-test).

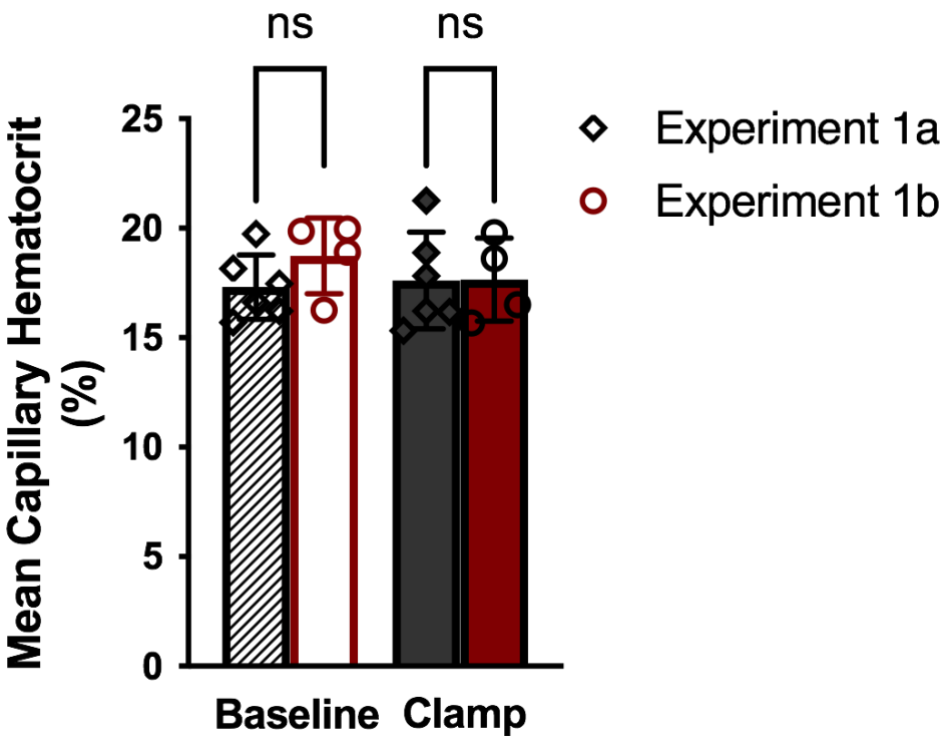

Figure 2.9 Mean capillary hematocrit measured during baseline and euglycemic clamp. Measurements of capillary hematocrit were taken in the extensor digitorum longus muscle, with Experiment 1a consisting of baseline and hyperinsulinemic euglycemic conditions and Experiment 1b consisting of baseline and sham clamp conditions (using saline). Each data point represents a per animal mean and error bars showing standard error of the mean. For 1a, hematocrit was 17% at baseline and 18% at hyperinsulinemic euglycemia ($p = 0.01$). N = 6 animals (677 capillaries at baseline, and 552 capillaries at clamp). For 1b, hematocrit was 19% at baseline and 18% following saline infusion. N = 4 animals (501 capillaries at baseline, and 417 capillaries at clamp).

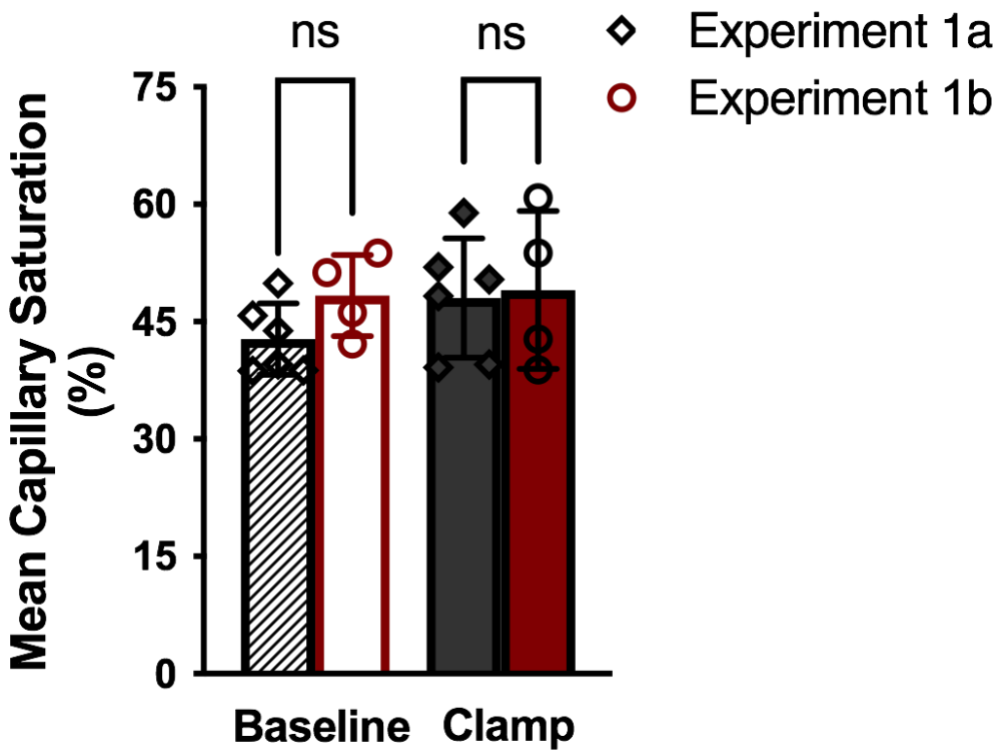

Figure 2.10 Mean red blood cell oxygen saturation measured during baseline and euglycemic clamp. Measurements of capillary red blood cell oxygen saturation were taken in the extensor digitorum longus muscle, with Experiment 1a consisting of baseline and hyperinsulinemic euglycemic conditions and Experiment 1b consisting of baseline and sham clamp conditions (using saline). Each data point represents a per animal mean and error bars showing standard error of the mean. For experiment 1a, SO_2 was 43% at baseline and 48% at hyperinsulinemic euglycemia. (N = 6 animals (659 capillaries at baseline, and 528 capillaries at clamp). For 1b, SO_2 was 48% at baseline and 49% following saline infusion. N = 4 animals (464 capillaries at baseline, and 397 capillaries at clamp).

2.3.3. Results: Experiment 2

For Experiment 2, 313 capillaries were analyzed at baseline conditions and 195 were analyzed at euglycemia across 6 animals for hemodynamic parameters. Under baseline conditions, mean RBC velocity was 217.7 ± 72.7 μm/sec during the initial 7% O_2 concentration. Velocity was significantly different at 12% and 2% concentrations, 177.9 ± 72.7 μm/sec ($p = 0.002$) and 273.4 ± 69.6 μm/sec ($p = 0.01$) respectively, under baseline conditions. For the final 7% concentration, mean velocity was 230.3 ± 76.3 μm/sec ($p = 0.03$). During euglycemia, mean RBC velocity was 235.4 ± 72.3 μm/sec during the initial 7% concentration. At 12% and 2% O_2 concentrations at euglycemia, mean velocity was 184.8 ± 56.9 and 271.9 ± 65.8 μm/sec respectively. For the final 7% concentration, mean RBC velocity was 233.8 ± 68.4 μm/sec. Comparing the velocity at each step of the oscillation between baseline and during euglycemia, no significant differences were found (Figure 2.11).

Mean RBC supply rate during the first 7% O_2 concentration was 10.7 ± 5.3 cells/sec at baseline conditions. Supply rate was significantly different at 12% and 2% concentrations during baseline, 6.9 ± 5.2 ($p = 0.01$) and 17.3 ± 5.2 cells/sec ($p = 0.01$) respectively. At the final 7% concentration, mean supply rate was 12.4 ± 6.6 cells/sec. During euglycemia, mean RBC supply rate was 10.8 ± 3.0 cells/sec during the first 7% O_2 concentration. Mean supply rate was significantly different at 12% and 2% concentrations, 7.3 ± 2.3 ($p = 0.03$) and 16.0 ±. 5.2 cells/sec ($p = 0.04$) respectively, at euglycemia. During the final 7% concentration, mean supply rate was 10.9 ± 4.5 cells/sec. No significant differences were found when comparing the corresponding mean supply rates measured at each O_2 concentration between the two conditions (Figure 2.12).

During baseline conditions, mean hematocrit was 12.3 ± 6.7% during the initial 7 concentration. At 12% and 2% O_2 concentrations, hematocrit was 11.8 ± 4.4 and 20.8 ± 1.8% respectively. Mean hematocrit at the final 7% concentration at baseline was 17.6 ± 2.6%. During euglycemia, mean hematocrit during the first 7% concentration was 10.4 ± 4.9%. Mean hematocrit was 12.9 ± 3.0 and 18.5 ± 4.3% at 12% and 2% concentrations respectively. During the final 7% concentration, mean hematocrit was 14.5 ± 3.8% at euglycemia. No significant differences were found between the two conditions when comparing the mean hematocrit at each step of the oxygen oscillation (Figure 2.13).

For saturation measurements, 110 capillaries were analyzed at baseline and 73 were analyzed at euglycemic conditions across 6 animals. At baseline conditions, mean SO_2 during the first 7% O_2 concentration was 60.4 ± 4.0%. Mean SO_2 significantly changed at 12% and 2% concentrations, 81.1 ± 4.1 ($p < 0.0001$) and 41.1 ± 5.3% ($p = 0.02$), at baseline. During the final 7% concentration, mean SO_2 was 63.1 ± 3.2%. At euglycemia, mean SO_2 was 60.8 ± 5.2% during the initial 7% concentration. Mean SO_2 significantly changed at 12% and 2% concentrations, 79.2 ± 6.4 ($p = 0.0004$) and 36.7 ± 6.6 ($p = 0.002$), during euglycemia. At the final 7% concentration, mean SO_2 was 56.3 ± 3.0%. When comparing the mean SO_2 across the oscillation between baseline and euglycemia, no significant differences were found (Figure 2.14).

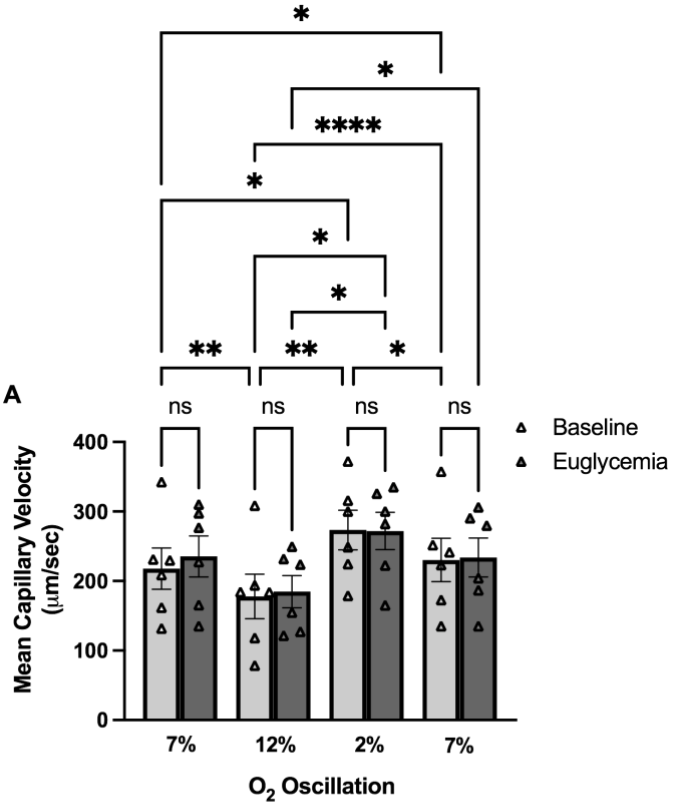
A
*
*
****
*
*
*
*
**
**
*
ns
ns
ns
ns
Baseline
Euglycemia
Mean Capillary Velocity (μm/sec)
400
300
200
100
0
7%
12%
2%
7%
O2 Oscillation

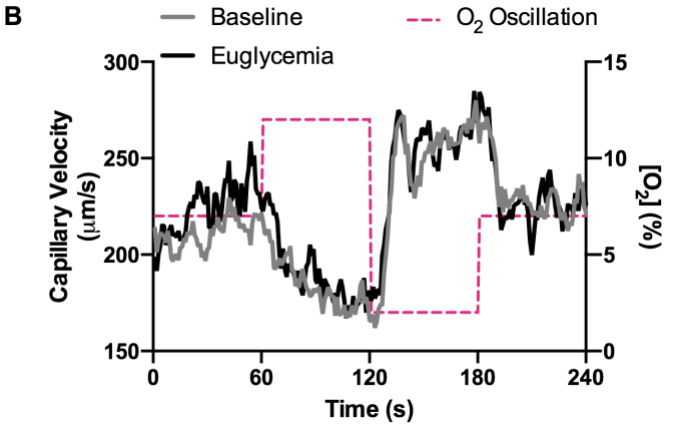
B
Baseline
O2 Oscillation
Euglycemia
Capillary Velocity (μm/s)
300
250
200
150
15
10
5
0
[O2] (%)
0
60
120
180
240
Time (s)

Figure 2.11 Mean capillary red blood cell velocity in response to oxygen oscillation during baseline and hyperinsulinemia euglycemic conditions in Experiment 2. A) Capillary red blood cell velocity measurements were made from intravital video microscopy sequences captured while the muscle was coupled with the gas exchange chamber microscope insert. O_2 concentrations ($[O_2]$) were oscillated from 7%-12%-2%-7% for 1 minute each in both conditions. The mean values represent the average of the last 15s of each 1 minute interval, compared to the 1 minute mean of the initial 7% chamber oxygen concentration included. Each point represents a per animal mean, with error bars showing standard error of the mean. B) Time series graph showing the changes in red blood cell (RBC) velocity across the 4 minute O_2 oscillation. Mean values were calculated for each second across the 240 s oscillation from each capillary analyzed from the extensor digitorum longus muscle using intravital microscopy video sequences and custom MATLAB software. N = 6 animals (313 capillaries at baseline, and 195 capillaries at clamp). *: $p < 0.05$, **: $p < 0.01$, ****: $p < 0.0001$ (one-way ANOVA).

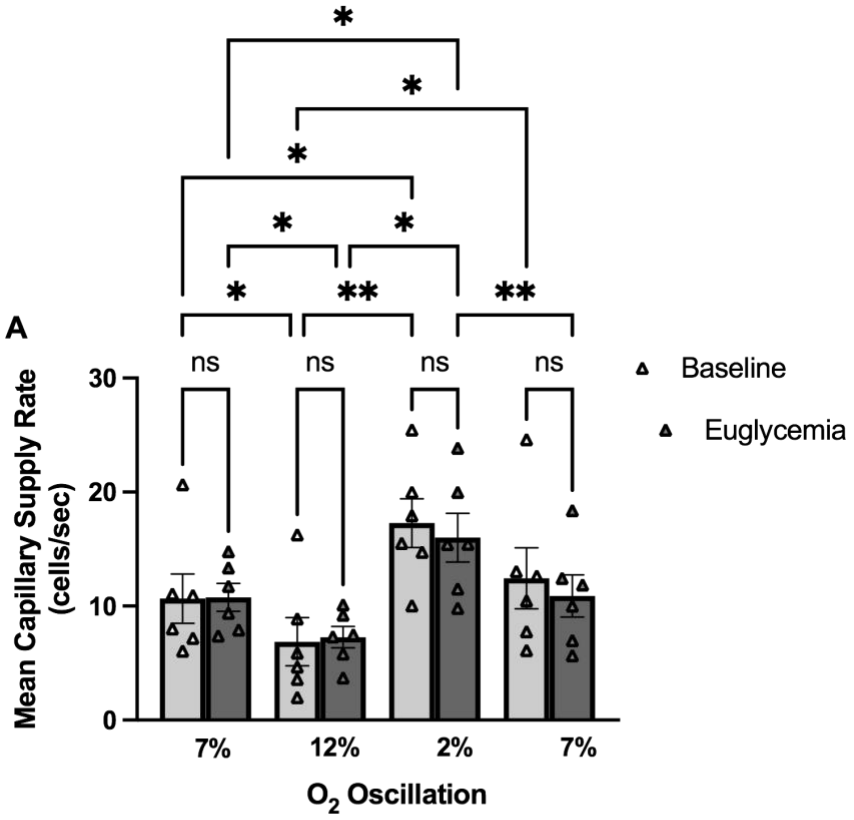
A
Mean Capillary Supply Rate (cells/sec)
30
20
10
0
ns
ns
ns
ns
*
*
*
*
*
*
**
**
Baseline
Euglycemia
7%
12%
2%
7%
O2 Oscillation

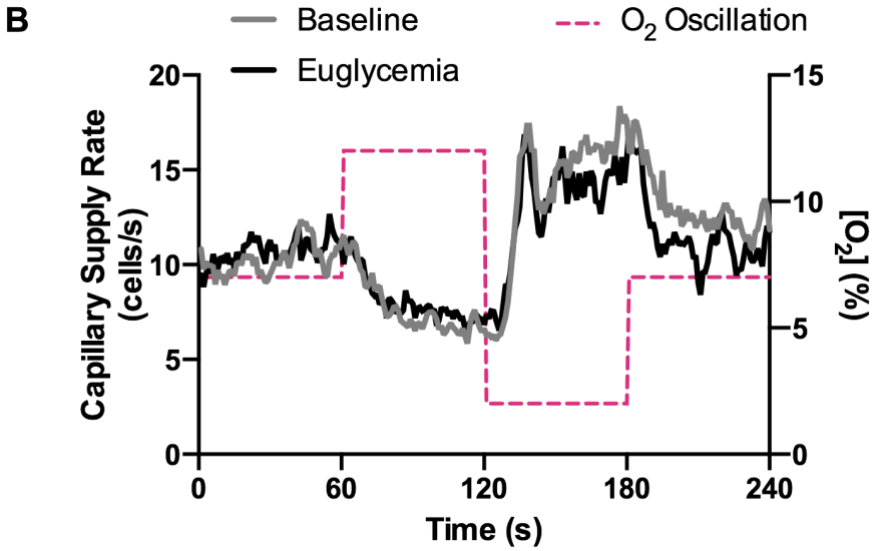
B
Baseline
Euglycemia
O2 Oscillation
Capillary Supply Rate (cells/s)
20
15
10
5
0
[O2] (%)
15
10
5
0
0
60
120
180
240
Time (s)

Figure 2.12 Mean capillary red blood cell supply rate in response to oxygen oscillation during baseline and hyperinsulinemia euglycemic conditions in Experiment 2. A) Capillary red blood cell supply rate measurements were made from intravital video microscopy sequences captured while the muscle was coupled with the gas exchange chamber microscope insert. O_2 concentrations ($[O_2]$) were oscillated from 7%-12%-2%-7% for 1 minute each in both conditions. The mean values represent the average of the last 15s of each 1 minute interval, compared to the 1 minute mean of the initial 7% chamber oxygen concentration included. Each point represents a per animal mean, with error bars showing standard error of the mean. B) Time series graph showing the changes in red blood cell (RBC) supply rate across the 4 minute O_2 oscillation. Mean values were calculated for each second across the 240 s oscillation from each capillary analyzed from the extensor digitorum longus muscle using intravital microscopy video sequences and custom MATLAB software. N = 6 animals (313 capillaries at baseline, and 195 capillaries at clamp). *: $p < 0.05$, ** $p < 0.01$ (one-way ANOVA).

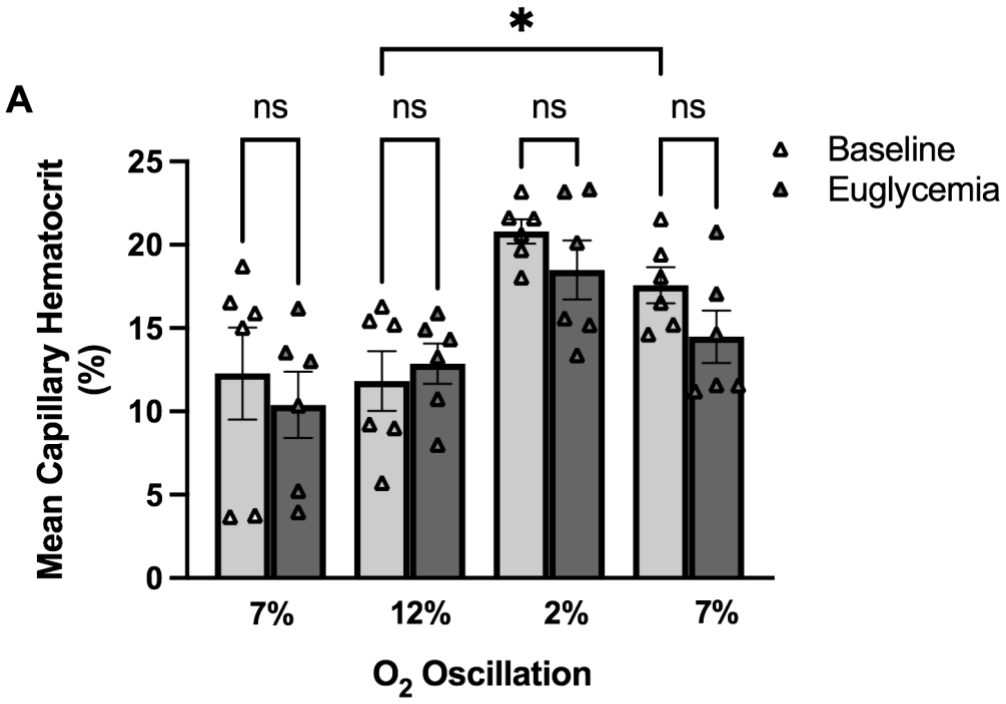
A
*
ns
ns
ns
ns
Baseline
Euglycemia
Mean Capillary Hematocrit (%)
25
20
15
10
5
0
7%
12%
2%
7%
O2 Oscillation

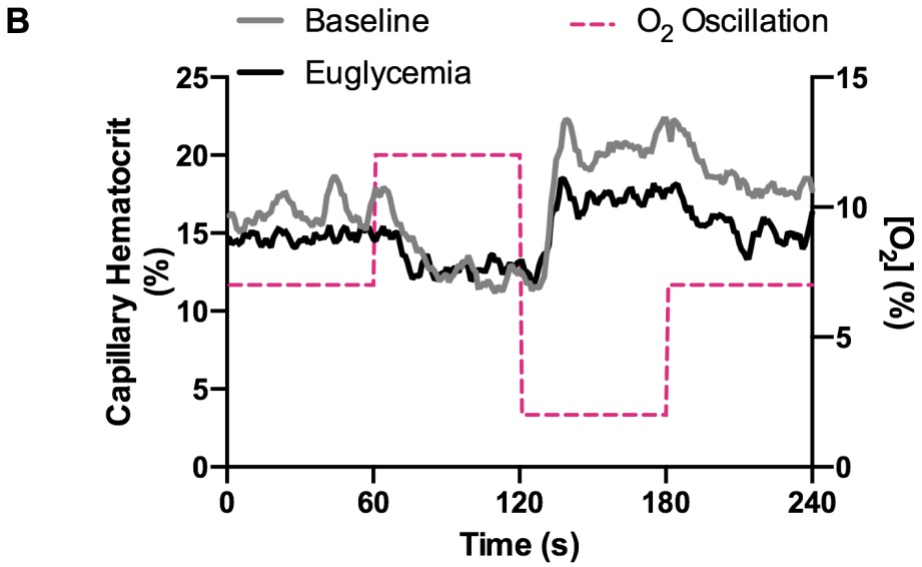
B
Baseline
O2 Oscillation
Euglycemia
Capillary Hematocrit (%)
25
20
15
10
5
0
15
10
5
0
[O2] (%)
0
60
120
180
240
Time (s)

Figure 2.13 Mean capillary hematocrit in response to oxygen oscillation during baseline and hyperinsulinemia euglycemic conditions in Experiment 2. A) Capillary hematocrit measurements were made from intravital video microscopy sequences captured while the muscle was coupled with the gas exchange chamber microscope insert. O_2 concentrations ($[O_2]$) were oscillated from 7%-12%-2%-7% for 1 minute each in both conditions. The mean values represent the average of the last 15s of each 1 minute interval, compared to the 1 minute mean of the initial 7% chamber oxygen concentration included. Each point represents a per animal mean, with error bars showing standard error of the mean. B) Time series graph showing the changes in red blood cell (RBC) hematocrit across the 4 minute O_2 oscillation. Mean values were calculated for each second across the 240 s oscillation from each capillary analyzed from the extensor digitorum longus muscle using intravital microscopy video sequences and custom MATLAB software. N = 6 animals (313 capillaries at baseline, and 195 capillaries at clamp). *: $p < 0.05$ (one-way ANOVA).

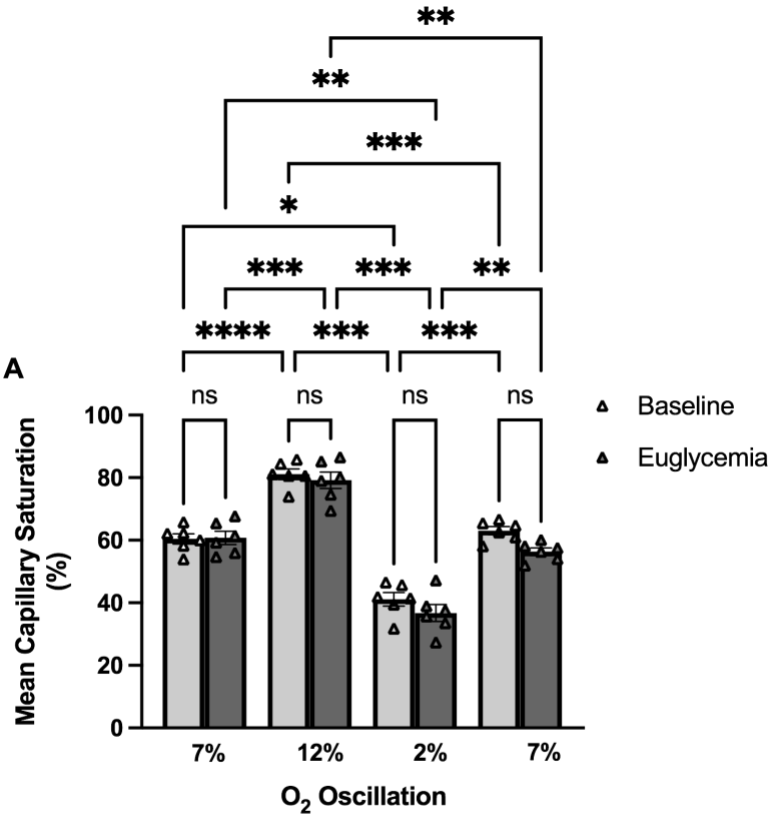
A
**
**
***
*
***
***
**
****
***
***
ns
ns
ns
ns
Mean Capillary Saturation (%)
100
80
60
40
20
0
7%
12%
2%
7%
O2 Oscillation
Baseline
Euglycemia

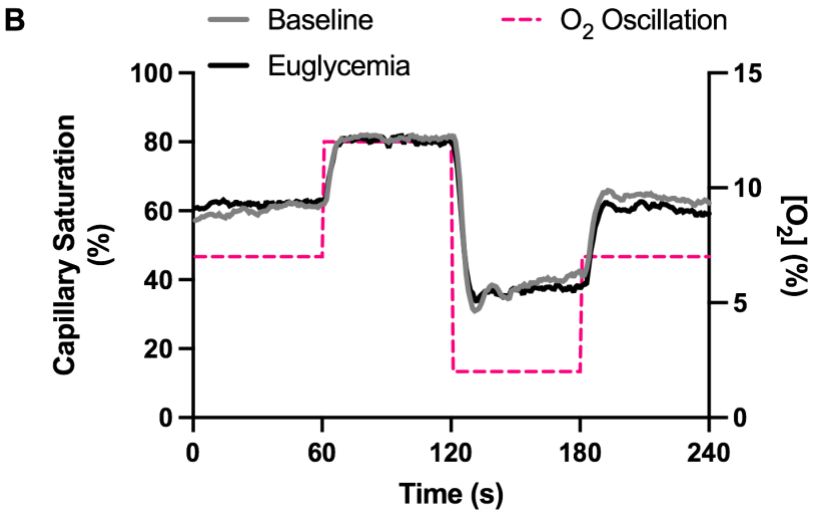
B
Baseline
Euglycemia
O2 Oscillation
Capillary Saturation (%)
100
80
60
40
20
0
15
10
5
0
[O2] (%)
0
60
120
180
240
Time (s)

Figure 2.14 Mean capillary red blood cell oxygen saturation in response to oxygen oscillation during baseline and hyperinsulinemia euglycemic conditions in Experiment 2. A) Capillary red blood cell oxygen saturation (SO_2) measurements were made from intravital video microscopy sequences captured while the muscle was coupled with the gas exchange chamber microscope insert. O_2 concentrations ($[O_2]$) were oscillated from 7%-12%-2%-7% for 1 minute each in both conditions. The mean values represent the average of the last 15 s of each 1 minute interval, compared to the 1 minute mean of the initial 7% chamber oxygen concentration included. Each point represents a per animal mean, with error bars showing standard error of the mean. Each point represents a per animal mean, with error bars showing standard error of the mean. B) Time series graph showing the changes in red blood cell (RBC) SO_2 across the 4 minute O_2 oscillation. Mean values were calculated for each second across the 240 s oscillation from each capillary analyzed from the extensor digitorum longus muscle using intravital microscopy video sequences and custom MATLAB software. N = 6 animals (110 capillaries at baseline, and 73 capillaries at clamp). *: $p < 0.05$, **: $p < 0.01$, ***: $p < 0.001$, ****: $p < 0.0001$ (one-way ANOVA).

2.4 Discussion

The objective of this study was to determine if skeletal muscle microvascular blood flow response to insulin is partially mediated by local tissue oxygen concentration. The first step to addressing this objective was to confirm previous observations that skeletal muscle microvascular blood flow increases in response to elevated blood insulin imposed via a hyperinsulinemic euglycemic clamp. In our experimental conditions, we found a significant increase in blood flow, determined by RBC supply rate, during hyperinsulinemic euglycemia (Experiment 1a; Figure 2.7). RBC supply rate significantly increased by 60% following the insulin infusion. This result matches the 80% increase observed by Akerstrom et al. (2019) using a similar animal model and method, and the 130% increase in femoral vein flow that Steinberg et al. (1994) measured in humans using an invasive thermodilution method. The different magnitude in the blood flow responses observed in our study are likely due to our methodology. Previous work has demonstrated that variations to the hyperinsulinemic euglycemic clamp method itself, such as decreasing the timeframe for infusion of insulin, will not provoke a significant change in blood flow due to insufficient time for the insulin mediated response (Vincent et al., 2004). In the present study, insulin was infused on average for 90 minutes before any measurements were taken, ensuring that sufficient time elapsed for insulin to elicit a response. Also, the anaesthetic employed in animal models could affect the baseline blood flow and the relative flow response to insulin. For example, sodium pentobarbital, used in the present study, is known to depress the central nervous system thus lowering basal sympathetic tone. This effect could explain, at least partially, the increased dilatation in arterioles and increase in blood flow (Shimokawa et al., 1998). Nevertheless,

we observed a significant increase in response to insulin despite having a higher supply rate measurement at baseline conditions. The findings from Experiment 1a were further supported from the lack of blood flow response observed in the sham euglycemic clamp employed in Experiment 1b.

A significant increase in supply rate measurements after performing the hyperinsulinemic euglycemic clamp confirms that insulin does increase blood flow in the skeletal muscle. The presence of normoglycemic blood levels, despite the continuous infusion during the clamp procedure, indicates that the high insulin also increases glucose uptake. Increases in blood flow in the microcirculation, even independently of insulin, have been shown to increase the delivery and therefore the uptake of glucose in the muscle tissue. Therefore, the increase in blood flow in response to high insulin levels further increases the insulin's ability to enhance glucose disposal from the blood (Baron et al., 1994; McClatchey et al., 2019). Glucose is transported throughout the body through the plasma, and Akerstrom et al. (2019) demonstrated that plasma flow, not just RBC flow, increased following insulin infusion, providing further evidence that insulin facilitates the glucose delivery and uptake in muscle tissue. Insulin is thought to increase skeletal muscle blood flow through modulation of NO release from the endothelial cells, causing vasodilation of arterioles increasing the blood flow in the microvasculature, and simultaneously increasing GLUT4 translocation to the cell surface in myocytes (Steinberg et al., 1994; Bhattacharya et al., 2007). Higaki et al. (2001) demonstrated that vasodilation caused by the NO production independent of insulin release, increased blood flow in skeletal muscle and therefore enhanced the glucose uptake. Consequently, there is strong evidence demonstrating that regulation of glucose by the insulin in the body is a

two-fold response: it increases blood flow to skeletal muscle to increase glucose availability in the microcirculation while simultaneously increasing GLUT4 translocation to the cell surface, both of which facilitate glucose uptake into the muscle tissue for metabolic processes.

In experiment 2, using the gas exchange chamber, hyperinsulinemic euglycemic clamp, and IVVM apparatus, we could measure the blood flow hemodynamics in the EDL microcirculation while simultaneously manipulating both insulin levels and oxygen concentrations. We found that the supply rate responded to the changing oxygen concentrations in the gas exchange chamber as expected, thus confirming that blood flow matches the oxygen conditions in the muscle tissue (Figure 2.7). Increasing oxygen concentrations to 12% in the chamber caused a decrease in blood flow, and the opposite occurred when the chamber dropped to a low oxygen concentration of 2% with nearly identical magnitude between baseline and euglycemic clamp conditions. In contrast to the results of Experiment 1a, an increase in blood flow was not observed during hyperinsulinemic conditions compared to the corresponding oxygen condition during baseline, showing that when the muscle is exposed to a fixed oxygen concentration, insulin no longer increases blood flow. This result suggests that the response due to insulin, at least partly, occurs in order to ensure sufficient O_2 delivery for glucose fixation. Therefore, when O_2 is being supplemented from another source, in this case the gas exchange chamber, insulin no longer stimulates an increase in skeletal muscle blood flow. Previous evidence demonstrating the impact of increased blood flow in the microcirculation on glucose uptake in skeletal muscle, combined with the results of our study, suggest that insulin increases blood flow to facilitate the delivery of both glucose

and oxygen to muscle tissue (Baron et al., 1994; McClatchey eet al., 2019). Our results from Experiment 2 are consistent with the suggestion made by Wilson and Matchinsky that sufficient oxygen levels must be maintained for muscle tissue to uptake glucose, a conclusion derived from computational modelling (Wilson & Matchinsky, 2019). Additionally, Experiment 2 demonstrates the effectiveness of combining a gas exchange device with IVVM to directly manipulate microvascular flow *in vivo* under a range of physiological conditions; future studies could be conducted to further investigate potential common mechanisms between O_2 and insulin in regulating blood flow, such as NO. A mechanism that links O_2 and insulin could explain the results of the present study and previous work showing a connection between NO release, both insulin and oxygen blood flow responses, and glucose uptake (Steinberg et al., 1994; Higaki et al., 2001; Golub et al., 2014).

The changes in both velocity and supply rate in the capillaries following the imposed O_2 changes as demonstrated in the time series plots provides clear evidence of the rapid and dynamic responses of the microcirculation to changing oxygen concentrations in muscle tissue (Figures 2.6 and 2.7). The SO_2 measurements show an almost instantaneous change in capillary RBC SO_2 in the muscle resulting from the imposed O_2 concentrations in the gas exchange chamber, with the hemodynamic parameters responding very shortly after. This is one of the few studies conducted that directly measures the effects of imposing SO_2 changes on blood flow in the microcirculation (Ghonaim, et al., 2011; Sové et al., 2021). The present study directly shows the effects of oxygen availability on flow to the muscle tissue, but previous methods studying blood flow in the microcirculation have often made conclusions based

on indirect observations. Changes in arteriolar diameter is frequently used to study changes in microvascular flow; an increase in diameter implicitly causes an increase in flow to downstream microvessels and vice versa (Tyml & Budreau, 1998; Jackson et al., 2010). However, increasing the diameter of a selected arteriole only increases blood flow entering the connected capillary bed downstream and does not represent an increase in total blood flow entering the microcirculation; this is due to the redistribution of blood flow that occurs in skeletal muscle to match metabolic demand when the entire cardiovascular tree is involved, therefore only measuring a single arteriole may not accurately reflect total blood flow changes in the microcirculation (Segal, 2005). Thus, being able to directly measure the change in hemodynamic parameters following the imposed SO_2 provides critical detail to quantify the dynamic effect that oxygen has on local blood flow regulation in the microcirculation.

The gas exchange chamber design and oxygen oscillation method used in this study was adapted from previous work and is an emerging method of directly manipulating RBC SO_2 in the microcirculation *in vivo* (Sové et al., 2021). Sové et al. (2021) imposed O_2 oscillations from 5%-12%-2%-5% and yet held the 12% and 2% O_2 chamber concentrations for 2 minutes opposed to 1 minute as in the present study. Additionally, in our study a single exchange window of approximately 5 x 3.5 mm in size was used to perturb a large area of the muscle tissue environment, but Sové et al. (2021) used an exchange device that consisted of five 200 x 400 um exchange windows interfaced with the muscle to study more localized effects of oxygen perturbations. Despite these technical differences, similar SO_2 levels were found across the oscillation in the selected capillaries in both studies, and this was irrespective of circulating insulin

levels as demonstrated in the present study. It has been suggested that RBCs are responsible for sensing low oxygen concentrations in the muscle environment through ATP release when hemoglobin desaturates in response to low oxygen conditions, which induces an increase in flow to the muscle (Ellsworth et al., 2016); at high oxygen concentrations, superoxide anions are generated in the interstitial space and are believed to neutralize NO, therefore negating its vasodilatory effects and reducing flow (Golub et al., 2014). The deoxygenation of hemoglobin has also been linked to the release of NO to stimulate vasodilation (Stambler et al., 1997). Oxygen binding to hemoglobin promotes the binding of NO to cysteineβ93 to form S-nitrohemoglobin, however during low oxygen conditions, S-nitrohemoglobin transitions from its R to its T structure, releasing NO in the process, resulting in an increase of blood flow and oxygen delivery to the muscle tissue (Stambler et al., 1997). Impairments in both ATP release from RBCs and insulin-induced eNOS phosphorylation to produce NO has been demonstrated previously in hyperinsulinemic conditions associated with insulin resistant diseases (Hanson et al., 2009; Hanson et al., 2010; Sprague et al., 2011; Kubota et al., 2011); however, there is no evidence that oxygen sensing is impaired in the present study, at either high, low, or normal oxygen concentrations. SO_2 measurements responded rapidly to the imposed oxygen perturbations in both baseline and euglycemic conditions, as demonstrated in the time transient data (Figure 2.13).

O_2 gas concentrations in the exchange chamber ranging from 2% - 12% have been used previously and were selected for several reasons (Ghonaim, et al., 2011). Mean tissue PO_2 in rat skeletal muscle is generally reported to be ~40mmHg (equivalent to ~5% [O_2]) and has been used in previous gas exchange studies (Sové et al., 2021). In our setup,

there is expected to be a small PO_2 drop across the gas exchange membrane and so we use a slightly higher [O_2] of 7% to maintain normal tissue PO_2. The low [O_2] of 2% (~15mmHg) is consistent with lower bounds of normal tissue PO_2, and importantly is above recent empirical measures of $P_{critical}$, below which mitochondrial respiration rates are likely to be affected (Golub & Pittman, 2012; Wilson, et al., 2014). High [O_2] at 12% (91mmHg) is consistent with arterial SO_2 (~93% saturation) allowing for RBC in capillaries to be highly saturated while remaining within a physiological range (Padilla, et al., 2007). 7% O_2 falls in the middle of the high and low concentrations chosen and therefore produces a balanced square wave oscillation allowing us to examine blood flow responses across a wide physiological range. This, however, results in a slightly higher baseline SO_2 in Experiment 2 compared to Experiments 1a and 1b. Baseline SO_2 measurements for Experiment 1a and 1b were 43% and 45% respectively, whereas baseline SO_2 at 7% O_2 was 60% (Figures 2.10 and 2.14). We would not expect that this difference in capillary SO_2 to impact our findings, as evidenced by the close matching in capillary RBC velocity and SR between baseline and euglycemic clamp at all three [O_2] studied.

Based on previous work by DeFronzo et al. (1979) and data gathered from the present study, there is evidence that glucose uptake and tissue metabolism are increased following the euglycemic clamp. DeFronzo et al. (1979) demonstrated that the glucose infusion rate at euglycemia is representative of glucose uptake, primarily occurring in skeletal muscle, and this increase in metabolism should result in an increase in oxygen consumption in the skeletal muscle based on the need for both oxygen and glucose to produce ATP through aerobic respiration (Wilson & Matchinsky, 2019). Further data

analysis measuring the extractions ratios of O_2 from the arterial to the venule end of the capillaries (as described previously) could be used to confirm that O_2 consumption is increased to accommodate changing myocyte glucose metabolism from the infusion of insulin (Ellis et al., 2002). Additionally, it should be noted that CO_2 concentrations were necessarily clamped at a steady 5% throughout all oxygen oscillations performed in the present study. CO_2 is a waste product produced from cellular processes in muscle tissue and also acts as a vasoactive stimulus; increased levels of CO_2 in the blood induce an increase in flow to the microcirculation through arteriole vasodilation to quickly dispose of this product of aerobic metabolism (Diji, 1959; Battisti-Charbonney et al., 2011). Therefore, clamping this vasoactive stimulus may also have an effect on blood flow responses in the present study. Maintaining CO_2 at 5% (~40 mmHg) is generally considered to be the normal physiological level and is consistent with other similar studies using both gas exchange chambers and superfusion solutions. Future studies could employ different CO_2 concentrations to confirm that clamping CO_2 at this level did not significantly affect the results found, although it is impossible to study one stimulus (i.e. O_2 or CO_2) without clamping the other due to the nature of the gas exchange chamber.

This study recapitulated that hyperinsulinemia increases blood flow in skeletal muscle microvasculature, and further demonstrated that setting the oxygen environment surrounding the muscle tissue also leads to a matching in blood flow to the imposed oxygen condition, irrespective of a hyperinsulinemic euglycemic condition. Finally, this study demonstrates for the first time a potential link between oxygen sensing and the hyperemic insulin response, as constraining the tissue oxygen concentration eliminated the expected hyperinsulinemic flow response, providing support for the hypothesis of this

study and changing our understanding of the interrelated effects of these stimuli on the microcirculation.

Perspectives

The use of a gas exchange chamber, coupled with IVVM, allows for the observation of direct effects of both insulin and oxygen on skeletal muscle microvasculature *in vivo*. The present study demonstrates for the first time a potential link between the blood flow responses to insulin and oxygen, specifically that constraining tissue oxygen concentration overrides insulin mediated hyperemia. This finding provides further insight into blood flow regulation and glucose disposal in skeletal muscle in healthy states which may ultimately inform our understanding in pathological conditions, such as insulin resistance and type 2 diabetes. This novel observation has potential implications for associated cardiovascular disease in which regulation of blood flow to match supply and demand of oxygen in muscle tissue is likely impaired.

Acknowledgments

We thank MUN Med3D for providing 3D printing services to build our device, the Canadian Institutes of Health Research for providing funding (CIHR PJT-162199), Drs. Reza Tabrizchi and Bruno Stuyvers for their advice on experimental design.

References

Akerstrom, T., Goldman, D., Nilsson, F., Milkovich, S. L., Fraser, G. M., Brand, C. L., et al. (2019). Hyperinsulinemia does not cause de novo capillary recruitment in rat skeletal muscle. *Microcirculation*, 1985(104), 889. http://doi.org/10.1111/micc.12593

Balon, T. W., & Nadler, J. L. (1997). Evidence that nitric oxide increases glucose transport in skeletal muscle. *Journal of Applied Physiology*, 82(1), 359–363. http://doi.org/10.1152/jappl.1997.82.1.359

Baron, A. D., Steinberg, H., Brechtel, G., & Johnson, A. (1994). Skeletal muscle blood flow independently modulates insulin-mediated glucose uptake. *American Journal of Physiology-Endocrinology and Metabolism*, 266(2), 248–253. http://doi.org/10.1152/ajpendo.1994.266.2.E248

Battisti‐Charbonney, A., Fisher, J., & Duffin, J. (2011). The cerebrovascular response to carbon dioxide in humans. *The Journal of Physiology*, 589(12), 3039-3048. https://dx.doi.org/10.1113%2Fjphysiol.2011.206052

Bhattacharya, S., Dey, D. & Roy, S.S. (2007). Molecular mechanism of insulin resistance. *J. Biosci*. 32(2): 405–413. doi:10.1007/s12038-007-0038-8.

DeFronzo, R.A., Tobin, J.D. & Andres, R. (1979). Glucose clamp technique: a method for quantifying insulin secretion and resistance. *Am. J. Physiol. Metab*, 237(3): 214- 213. doi:10.1152/ajpendo.1979.237.3.

Diji, A. (1959). Local vasodilator action of carbon dioxide on blood vessels of the hand. *Journal of Applied Physiology*, 14(3), 414-416. https://doi.org/10.1152/jappl.1959.14.3.414

Ellis, C.G., Ellsworth, M.L. & Pittman, R.N. (1990). Determination of red blood cell oxygenation in vivo by dual video densitometric image analysis. *Am. J. Physiol,* 258(4): 1216-1223. doi:10.1152/ajpheart.1990.258.4.

Ellis, C.G., Ellsworth, M.L., Pittman, R.N., & Burgess, W.L. (1992). Application of image analysis for evaluation of red blood cell dynamics in capillaries. *Microvascular Research*, 44(2):214-225. doi:10.1016/0026-2862(92)90081-Y.

Ellis, C.G., Bateman, R.M., Sharpe, M.D., Sibbald, W.J., Gill., R. (2002). Effect of maldistribution of microvascular blood flow on capillary O_2 extraction in sepsis.

American Journal of Physiology Heart and Circulatory Physiology, 282, H156-H164. https://doi.org/10.1152/ajpheart.2002.282.1.h156

Ellsworth, M. L., Ellis, C. G. & Sprague, R. S. (2016). Role of erythrocyte-released ATP in the regulation of microvascular oxygen supply in skeletal muscle. *Acta Physiologica*, 216(3), 265-276. https://doi.org/10.1111/apha.12596

Fraser, G.M., Milkovich, S., Goldman, D., & Ellis, C.G. (2012b). Mapping 3-D functional capillary geometry in rat skeletal muscle in vivo. *American Journal of Physiology Heart and Circulatory Physiology*, 302(3):H654-664. https://doi.org/10.1152/ajpheart.01185.2010

Ghonaim, N.W., Lau, L.W.M., Goldman, D., Ellis, C.G., & Yang, J. (2011). A micro-delivery approach for studying microvascular responses to localized oxygen delivery. *Microcirculation,* 18, 646-654. https://dx.doi.org/10.1111%2Fj.1549-8719.2011.00132.x

Golub, A.S. and R.N. Pittman. (2012). Oxygen dependence of respiration in rat spinotrapezius muscle in situ. *Am J Physiol Heart Circ Physiol*, 303(1), 47-56. https://doi.org/10.1152/ajpheart.00131.2012

Golub, A. S., Song, B. K., & Pittman, R. N. (2014). Muscle contraction increases interstitial nitric oxide as predicted by a new model of local blood flow regulation. *The Journal of Physiology*, 592(6), 1225-1235. https://doi.org/10.1113/jphysiol.2013.267302

Hanson, M. S., Ellsworth, M. L., Achilleus, D., Stephenson, A. H., Bowles, E. A., Sridharan, M., Adder- ley, S. & Sprague, R. S. (2009). Insulin inhibits low oxygen-induced ATP release from human erythrocytes: implication for vascular control. *Microcirculation,* 16, 424–433. https://dx.doi.org/10.1080%2F10739680902855218

Hanson, M. S., Stephenson, A. H., Bowles, E. A. & Sprague, R. S. (2010). Insulin inhibits human erythrocyte cAMP accumulation and ATP release: role of phosphodiesterase 3 and phosphoinositide 3- kinase. *Exp. Biol. Med*, 235, 256–262. https://doi.org/10.1258/ebm.2009.009206

Higaki, Y., Hirshman, M. F., Fujii, N., & Goodyear, L. J. (2001). Nitric oxide increases glucose uptake through a mechanism that is distinct from the insulin and contraction pathways in rat skeletal muscle. *Diabetes*, 50(2), 241–247. http://doi.org/10.2337/diabetes.50.2.241

Hudlicka, O. (1985). Regulation of muscle blood flow. *Clin Physiol,* 5:201–229.

Jackson, D. N., Moore, A. W., & Segal, S. S. (2010). Blunting of rapid onset vasodilatation and blood flow restriction in arterioles of exercising skeletal muscle with ageing in male mice. *The Journal of Physiology*, 588(12), 2269-2282. https://doi.org/10.1113/jphysiol.2010.189811

Japee, S. A., Ellis, C. G., & Pittman, R. N. (2004). Flow Visualization Tools for Image Analysis of Capillary Networks. *Microcirculation*. 11, 39-54. doi:10.1080/10739680490266171.

Kubota, T., Kubota, N., Kumagai, H., Yamaguchi, S., Kozono, H., Takahashi, T., . . . Kadowaki, T.. (2011). Impaired Insulin Signaling in Endothelial Cells Reduces Insulin-Induced Glucose Uptake by Skeletal Muscle. *Cell Metabolism*, 13(3), 294-307. https://doi.org/10.1016/j.cmet.2011.01.018

Leonard, B.L., Watson, R.N., Loomes, K.M., Phillips, A.R.J., & Cooper, G.J. (2005). Insulin resistance in the Zucker diabetic fatty rat: a metabolic characterisation of obese and lean phenotypes. *Acta Diabetologica*, 42, 162-170. https://doi.org/10.1007/s00592-005-0197-8

McClatchey, P. M., Williams, I. M., Xu, Z., Mignemi, N. A., Hughey, C. C., McGuinness, O. P., et al. (2019). Perfusion controls muscle glucose uptake by altering the rate of glucose dispersion in vivo. *American Journal of Physiology-Endocrinology and Metabolism*, 317(6), 1022–1036. http://doi.org/10.1152/ajpendo.00260.2019

Merry, T. L., Steinberg, G. R., Lynch, G. S., & McConell, G. K. (2010). Skeletal muscle glucose uptake during contraction is regulated by nitric oxide and ROS independently of AMPK. *American Journal of Physiology-Endocrinology and Metabolism*, 298(3), 577–585. http://doi.org/10.1152/ajpendo.00239.2009

Padilla, D. J., McDonough, P., Behnke, B. J., Kano, Y., Hageman, K. S., Musch, T. I., & Poole, D. C. (2007) Effects of Type II diabetes on muscle microvascular oxygen pressures. *Respir Physiol Neurobiol*, 156(2), 187-195. doi: 10.1016/j.resp.2006.08.008.

Sandstrom, M. E., Zhang, S., Briton, J., Silva, J. P., Reid, M. B., Westerblad, H., & Katz, A. (2006). Role of reactive oxygen species in contraction-mediated glucose transport in mouse skeletal muscle. *Journal of Physiologyi*, 575, 251-262. doi: 10.1113/jphysiol.2006.110601

Segal, S. (2005). Regulation of Blood Flow in the Microcirculation. *Microcirculation.* 12, 33-45. http://doi.org/10.1080/10739680590895028

Shimokawa, A., Kunitake, T., Takasaki, M., & Kannan, H. (1998). Differential effects of anesthetics on sympathetic nerve activity and arterial baroreceptor reflex in chronically instrumented rats. *Journal of the Autonomic Nervous System*, 72(1), 46-54. https://doi.org/10.1016/s0165-1838(98)00084-8

Sové, R. J., Milkovich, S., Nikolov, H., & Holdsworth, D. (2021). Localized oxygen exchange platform for intravital video microscopy investigations of microvascular oxygen regulation. *Frontiers in Physiology*, *12*, 505. https://doi.org/10.3389/fphys.2021.654928

Sprague, R. S., Bowles, E. A., Achilleus, D., Stephenson, A. H., Ellis, C. G. & Ellsworth, M. L. (2011). A selective phosphodiesterase 3 inhibitor rescues low PO_2-induced ATP release from erythrocytes of humans with type 2 diabetes: implication for vascular control. *Am J Physiol*, 301, H2466-H2472. https://doi.org/10.1152/ajpheart.00729.2011

Stamler, J. S., Jia, L., Eu, J. P., Mcmahon, T. J., Demchenko, I. T., Bonaventura, J., . . . Piantadosi, C. A. (1997). Blood Flow Regulation by S-Nitrosohemoglobin in the Physiological Oxygen Gradient. *Science (American Association for the Advancement of Science)*, 276(5321), 2034-2037. https://doi.org/10.1126/science.276.5321.2034

Steinberg, H. O., Brechtel, G., Johnson, A., Fineberg, N., & Baron, A. D. (1994). Insulin-mediated skeletal muscle vasodilation is nitric oxide dependent. A novel action of insulin to increase nitric oxide release. *The Journal of Clinical Investigation*, 94(3), 1172–1179. http://doi.org/10.1172/JCI117433

Tyml K., & Budreau, C.H. (1991). A new preparation of rat extensor digitorum longus muscle for intravital investigation of the microcirculation. *International Journal of Microcirculation, Clinical and Experimental*, 10(4):335-343.

Tyml, K., Yu, J., & McCormack, D. G. (1998). Capillary and arteriolar responses to local vasodilators are impaired in a rat model of sepsis. *Journal of Applied Physiology*. http://doi.org/10.1152/jappl.1998.84.3.837

Vincent, M. A., Clerk, L. H., Lindner, J. R., Klibanov, A. L., Clark, M. G., Rattigan, S., & Barrett, E. J. (2004). Microvascular recruitment is an early insulin effect that regulates skeletal muscle glucose uptake in vivo. Diabetes, 53(6), 1418–1423. http://doi.org/10.2337/diabetes.53.6.1418

Wilson, D.F., D.K. Harrison, and A. Vinogradov. (2014). Mitochondrial cytochrome c oxidase and control of energy metabolism: measurements in suspensions of isolated mitochondria. *J Appl Physiol*, 117(12),1424-1430. https://doi.org/10.1152/japplphysiol.00736.2014

Wilson, D. F., & Matschinsky, F. M. (2019). Oxygen dependence of glucose sensing: role in glucose homeostasis and related pathology. *Journal of Applied Physiology*, 126(6), 1746–1755. http://doi.org/10.1152/japplphysiol.00047.2019

Zierath, J R., & Krook, A. (2000). Insulin action and insulin resistance in human skeletal muscle. *Diabetologia*, 43, 821-835. https://doi.org/10.1007/s001250051457

Chapter 3: Summary

3.1 Summary and Discussion of Results

In Chapter 2, it was demonstrated through the first set of experiments (that in our hands insulin increases microvascular blood flow and stimulates glucose uptake during hyperinsulinemic euglycemic clamp (Objective 1). Both capillary red blood cell (RBC) velocity and supply rate increased significantly under euglycemia compared to baseline. This finding is consistent with what has been reported previously using similar methods in both animal and human studies. In contrast, our sham clamp Experiment 1b, did not produce a similar increase in flow compared to Experiment 1a. Experiment 1b showed no significant differences in capillary RBC velocity or supply rate between baseline measurements and measurements taken following the infusion of saline during the sham clamp; the absence of a flow response during the sham euglycemic clamp verifies that infusion of saline alone has no impact on microvascular blood flow, nor does the blood flow increase over time while the animal is maintained for intravital video microscopy (Objective #2). Finally, in Experiment 2, measured RBC oxygen saturation (SO_2) dynamically changed to match oxygen concentrations imposed by the gas exchange chamber as expected. SO_2 increased with increased oxygen concentrations and vice versa, in both baseline and euglycemic conditions. Additionally, capillary blood flow responded to the imposed O_2 changes in the gas exchange chamber as expected. Velocity and supply rate measurements significantly increased during low oxygen concentrations, and significantly decreased during high oxygen concentration in nearly identical proportions at baseline and euglycemic conditions. As such, no significant differences in capillary

supply rate were found between baseline and euglycemic conditions at corresponding oxygen concentrations, unlike what was found in Experiment 1a (Objective #3). Remarkably, capillary RBC supply rate measurements taken at baseline mirrored those taken during euglycemia matching across the entire oxygen oscillation (Figure 11, Chapter 2). The elimination of the insulin-mediated blood flow response seen in Experiment 2 is a novel finding and provides new information suggesting a link between insulin and oxygen blood flow regulation. Previously, it has been demonstrated that insulin increased blood flow to increase the delivery of glucose to skeletal muscle in order to facilitate glucose uptake, and this uptake requires the use of ATP which is produced from aerobic respiration (Steinberg et al., 1994; Ramos et al., 2020). The results from this thesis suggest that insulin may also increase blood flow to facilitate the delivery of oxygen to the muscle tissue as well to ensure enough energy is produced to convert glucose into glycogen, and when the tissue oxygen environment is clamped from another source, such as a gas exchange chamber, insulin no longer provokes an increase in flow to provide more oxygen to the muscle.

3.2 Limitations

The hyperinsulinemic euglycemic clamp has become a standard for measuring the effects of insulin on blood flow and glucose uptake in the body as well as an individual's sensitivity to the hormone (DeFronzo et al., 1979). This method has proven effective in a variety of different models, including both animal and human studies. In the present study, the blood flow response typically seen with an increase of insulin in the body was

directly measured in the skeletal muscle microcirculation, but glucose uptake and oxygen consumption of the surrounding muscle tissue was not directly measured. Blood glucose levels were continuously measured at regular intervals from a tail sample once the clamp was started and these measurements were used as an indicator of glucose uptake rate and metabolism. As insulin is steadily infused during the clamp, glucose is also infused at varying rates to maintain normoglycemia. Since high levels of both insulin and glucose are being infused into the animal subject, but blood glucose is maintained at a normal level, it can be deduced that the rate of glucose infusion matches that which is being metabolized in skeletal muscle tissue (DeFronzo et al., 1979). Additionally, if glucose uptake is increased to facilitate increased metabolism in the muscle, then we expect increased oxygen consumption may also have to occur, as aerobic respiration is the primary means through which muscle tissue at rest produces the ATP necessary for cellular processes such as glucose fixation.

Although the gas exchange chamber is an elegant tool for directly manipulating the oxygen concentrations in the muscle tissue environment, it does have limitations. During the oxygen oscillations, N_2 was automatically adjusted to balance the total gas composition, but CO_2 remained steady at a 5% concentration. This steady level of CO_2 in the chamber was chosen to maintain tissue PCO_2 at the expected physiological level of ~40 mmHg. However, the consequences of clamping muscle tissue at a specific CO_2 concentration on microvascular blood flow remains unknown. CO_2 is known to act as a vasoactive stimulus that can alter blood flow in the microcirculation through vasodilation of arterioles. An abundance of CO_2 in the capillary bed stimulates an increase of blood flow to the muscle tissue in order to accelerate the removal of CO_2, as it is a waste

product that is formed from cellular processes and excesses can cause an increase in tissue pH (Diji, 1959; Battisti-Charbonney, et al., 2011). Ongoing research within our lab group has demonstrated that the gas exchange chamber can also be used to perform CO_2 oscillations, similar to the O_2 oscillations performed in the present study, and these experiments have demonstrated that blood flow responds dynamically to CO_2 perturbations in a manner similar to O_2 perturbations. Although CO_2 was kept fixed in the study described in Chapter 2, microvascular blood flow showed profound responses to changing exchange chamber oxygen concentrations across the range imposed. Unravelling how both O_2 and CO_2 may work in concert to establish the level of capillary blood flow, both at rest and during hyperinsulinemia, is a topic for future study.

3.3 Future Directions

The outcome of the work for this thesis has provided evidence to support the hypothesis that insulin mediated hyperemia is partially dependent on local muscle oxygen concentration. In Experiment 1a, there were no significant differences in SO_2 measurements between baseline and euglycemic clamp conditions despite a significant increase in RBC supply rate at euglycemia. This finding suggests that more oxygen is being consumed by the muscle tissue during clamp conditions because more oxygen is being delivered from the increased blood flow to the muscle, but we are not seeing a subsequent increase in SO_2 measurements. In order to determine that oxygen consumption may increase during the hyperinsulinemic euglycemic clamp in conjunction with increased insulin-mediated glucose uptake, future studies can be undertaken to

calculate oxygen extraction ratios from the EDL capillaries as has been described previously (Ellis et al., 2002). This measurement represents the extraction of oxygen as it passes through the capillaries in the muscle by comparing the differences in capillary RBC O_2 saturation measurements at the arteriolar and venular end of the capillaries, which are weighed against RBC SR measurements in the corresponding capillaries to account for different rates of blood flow. The ratio between the saturation measurements taken at the opposite ends of the capillaries would increase if oxygen consumption in the muscle has increased, as this would indicate that more oxygen is being extracted from the capillaries into the muscle tissue and thus a much lower venule saturation measurement will be recorded, creating a bigger difference between the arterial and venule measurements compared to resting conditions where oxygen consumption rates would be lower. Increased blood flow will typically result in an increased venular saturation measurement under resting conditions, and under conditions with increased tissue metabolism, this will appear as a small difference between arterial and venule saturation, despite extraction having actually increased; the equation to calculate extraction ratios accounts for these scenarios by incorporating SR measurements taken at individual capillaries.

The combination of the hyperinsulinemic clamp, IVVM apparatus, and the gas exchange chamber allow for the direct observation of multiple stimuli interacting in the skeletal muscle simultaneously and can be adjusted to further study potential mediators involved in these interactions. The vasodilatory effects of insulin and the resulting increases in blood flow have been attributed to the release of NO from the endothelium and this mechanism has been studied extensively in the past (Wang et al., 2013; Steinberg

et al., 1994); more recently, however, NO release has been linked to glucose uptake in skeletal muscle and even O_2 consumption (Higaki et al., 2001; Golub et al., 2014). The effects of NO have been studied in various conditions using NO blockers such as L-NMMA to block the release of NO from the endothelial using the hyperinsulinemic euglycemic clamp (Steinberg et al., 1994). However, blocking NO has never been done while simultaneously infusing insulin and glucose using the clamp method while performing oxygen perturbations. The infusion of a NO blocker could be added to the methods already used in this thesis in order to further assess if the insulin-mediated blood flow response is partially dependent on local oxygen concentrations. Blocking the release of NO from the endothelium would give us the ability to study the oxygen-mediated blood flow responses and the subsequent interactions with insulin independently of the NO mechanism.

The methods employed in this thesis could easily be adapted to study blood flow regulation in disease models. The hyperinsulinemic euglycemic clamp is frequently used to study impairments in insulin-mediated blood flow responses and glucose uptake by comparing results healthy and insulin resistance models, such as a type 2 diabetic model (DeFronzo et al., 1979; Ramos et al., 2020). Direct observation of the microcirculation during oxygen perturbations using the IVVM apparatus and gas exchange device in an insulin resistant model could provide further insight into the impairments of blood flow regulation seen in these conditions, which are often associated with cardiovascular diseases. It is has been shown previously that insulin-mediated hyperaemia is eliminated in diabetic models, therefore the delivery of nutrients such as glucose and oxygen to skeletal muscle tissue in these models is impaired (Clerk et al., 2006); additional studies

have measured decreases in RBC velocity in diabetic models and further calculations predicted an approximate 50% decrease in oxygen delivery to skeletal muscle (Kindig et al., 1998).

Our research group has demonstrated that the gas exchange device can be used for both O_2 and CO_2 perturbations in the skeletal muscle microcirculation. To address one of the limitations of the present study, future work could perform O_2 oscillations at different physiological CO_2 concentrations to determine if tissue CO_2 concentration impacts the resulting blood flow responses to imposed O_2 changes. Hemodynamic measurements across the O_2 oscillation at high and low CO_2 concentrations can be compared against the measurements taken at the 5% CO_2 concentration, like in the present study, and any differences could be observed and quantified. However, it is important to note that when using the gas exchange chamber to study the effects of manipulating either O_2 or CO_2 on microvascular blood flow, the other gas has to be clamped in order to vary the concentration of the other; in other words, it is impossible to conduct O_2 perturbations without clamping CO_2 at some concentration, and vice versa. Taking this into consideration, it is very difficult to completely separate the influences these gases have on each other, and to study each stimulus completely independently. Despite this, insulin-mediated blood flow responses and glucose uptake could then also be compared across different CO_2 concentrations; this is a topic that has yet to be addressed in the literature and there could be an interaction between insulin and CO_2 in the microcirculation, like we saw with O_2, but it has not yet been studied.

3.4 Final Summary

The regulation of blood flow in the microcirculation is a dynamic process that ensures the supply of nutrients to muscle tissue matches the moment-to-moment aerobic demands of the parenchyma. This occurs through modulation of arteriolar vascular tone that can either contract or dilate in response to various vasoactive stimuli such as insulin and oxygen. The goal of this thesis was to quantify the capillary blood flow responses to both insulin and oxygen *in vivo* using a gas exchange device combined with IVVM and a hyperinsulinemic euglycemic clamp to address the following hypothesis: insulin-mediated blood flow increases are partially mediated by local oxygen concentrations. Three different experimental protocols were conducted in this thesis to address the hypothesis, starting with the first set of experiments that demonstrated in our hands using a hyperinsulinemic euglycemic clamp that hyperinsulinemia does increase blood flow in skeletal muscle microcirculation. The second set of experiments were conducted to support the use of the clamp method and demonstrated that blood flow did not increase from simply infusing saline or due to any time effects. Finally, the third set of experiments combined the gas exchange chamber with the hyperinsulinemic euglycemic clamp and we found that the insulin-mediated blood flow response was abolished when oxygen concentrations were clamped using the exchange device. The results gathered from these experiments provides the first evidence that skeletal muscle hyperemia caused by insulin may have an oxygen mediated component; this finding has wide ranging impact of our understanding of glucose disposal and how defects to oxygen mediated blood flow regulation may impact pathological states such as type 2 diabetes by further hampering glucose disposal.

References

Battisti-Charbonney, A., Fisher, J., & Duffin, J. (2011). The cerebrovascular response to carbon dioxide in humans. *The Journal of Physiology*, 589(12), 3039-3048. https://dx.doi.org/10.1113%2Fjphysiol.2011.206052

Clerk, L. H., Vincent, M. A., Jahn, L. A., Liu, Z., Lindner, J. R. & Barrett, E. J. (2006). Obesity Blunts Insulin-Mediated Microvascular Recruitment in Human Forearm Muscle. *Diabetes*, 55(5), 1436-1442. doi: 10.2337/db05-1373.

DeFronzo, R.A., Tobin, J.D. & Andres, R. (1979). Glucose clamp technique: a method for quantifying insulin secretion and resistance. Am. J. Physiol. Metab, 237(3): 214- 213. doi:10.1152/ajpendo.1979.237.3.

Diji, A. (1959). Local vasodilator action of carbon dioxide on blood vessels of the hand. Journal of Applied Physiology, 14(3), 414-416. https://doi.org/10.1152/jappl.1959.14.3.414

Ellis, C.G., Bateman, R.M., Sharpe, M.D., Sibbald, W.J., Gill., R. (2002). Effect of maldistribution of microvascular blood flow on capillary O2 extraction in sepsis. American Journal of Physiology Heart and Circulatory Physiology, 282, H156-H164. https://doi.org/10.1152/ajpheart.2002.282.1.h156

Golub, A. S., Song, B. K., & Pittman, R. N. (2014). Muscle contraction increases interstitial nitric oxide as predicted by a new model of local blood flow regulation. The Journal of Physiology, 592(6), 1225-1235. https://doi.org/10.1113/jphysiol.2013.267302

Higaki, Y., Hirshman, M. F., Fujii, N., & Goodyear, L. J. (2001). Nitric oxide increases glucose uptake through a mechanism that is distinct from the insulin and contraction pathways in rat skeletal muscle. Diabetes, 50(2), 241–247. http://doi.org/10.2337/diabetes.50.2.241

Kindig, C. A., Sexton, W. L., Fede, M. R., & Poole, D. C. (1998). Skeletal muscle microcirculatory structure and hemodynamics in diabetes. *Respiration Physiology*, 111(2), 163-175. https://doi.org/10.1016/S0034-5687(97)00122-9

Kubota, T., Kubota, N., Kumagai, H., Yamaguchi, S., Kozono., H., Takahashi, T., . . . Kadowaki, T. (2011). Impaired Insulin Signaling in Endothelial Cells Reduces Insulin-Induced Glucose Uptake by Skeletal Muscle. *Cell Metabolism*, 13(3), 294-307. https://doi.org/10.1016/j.cmet.2011.01.018

Ramos, P. A., Lytle, K. A., Delivanis, D., Nielsen, S., LeBrasseur, N. K., & Jensen, M. D. (2020). Insulin-Stimulated Muscle Glucose Uptake and Insulin Signaling in Lean

and Obese Humans. The Journal of Clinical Endocrinology and Metabolism, 1-16. doi: 10.1210/clinem/dgaa919.

Steinberg, H. O., Brechtel, G., Johnson, A., Fineberg, N., & Baron, A. D. (1994). Insulin-mediated skeletal muscle vasodilation is nitric oxide dependent. A novel action of insulin to increase nitric oxide release. *The Journal of Clinical Investigation*, 94(3), 1172–1179. http://doi.org/10.1172/JCI117433

Wang, H., Wang, A. X., Aylor, K., & Barrett, E. J. (2013). Nitric Oxide Directly Promotes Vascular Endothelial Insulin Transport. *Diabetes*, 62(12), 4030-4042. https://doi.org/10.2337/db13-0627

Appendix 1

Institutional Animal Care Committee (IACC)
St. John's, NL, Canada A1C 5S7
Tel: 709 777-6621 acs@mun.ca
www.mun.ca/research/about/acs/

March 8, 2018

Dear: Dr. Graham Fraser, Assistant Professor/Faculty of Medicine\Division of BioMedical Sciences

Researcher Portal File No.: 20170834
Animal Care File: 16-01-GF
Entitled: (16-01-GF) Microvascular Blood Flow, Regulation, and Insulin Sensitivity in Type 2 Diabetes
Status: Active

Approval Date: November 13, 2016
Annual Report Due: October 03, 2018
Ethics Clearance Expires: November 13, 2019

This is to confirm that your Animal Use Protocol application to engage in procedures involving animals was considered by the IACC, and approved on a 3-year term on November 13, 2016. A renewal is required after the ethics clearance expires on November 13, 2019.

An Event [Annual Report] will be required following each year of protocol activity.

Should you encounter an unexpected incident that negatively affects animal welfare or the research project relating to animal use, please submit an Event [Incident Report].

Any alterations to the protocol requires prior submission and approval of an Event [Amendment].

Sincerely,

ANULIKA MBAKWE | IACC COORDINATOR
Department of Animal Care Services
Memorial University of Newfoundland
Health Sciences Centre
Room H1848

Appendix 2

MEMORIAL UNIVERSITY
Animal Care Committee (ACC)
St. John's, NL, Canada A1C 5S7
Tel: 709 777-6620 acs@mun.ca
https://www.mun.ca/research/about/acs/acc/

November 13, 2019

Dear: Dr. Graham Fraser, Faculty of Medicine\Division of BioMedical Sciences

Researcher Portal File No.: 20200860
Animal Care File: 19-01-GF
Entitled: (19-01-GF) Microvascular Blood Flow, Regulation, and Insulin Sensitivity in Type 2 Diabetes
Status: Active

Approval Date: November 13, 2019
Annual Report Due: November 13, 2020
Ethics Clearance Expires: November 13, 2022

Your Animal Use Protocol (AUP) renewal application to engage in procedures involving animals has been approved for a three-year term. This AUP replaces the previous protocol [[16-01-GF]] as the active ethics clearance associated with this project. Please note the new AUP number when referring to this protocol.

This ethics clearance includes the following Team Members: Dr. Graham Fraser (Principal Investigator)

An Event [Annual Report] will be required following each year of protocol activity.

Should you encounter an unexpected incident that negatively affects animal welfare or the research project relating to animal use, please submit an Event [Incident Report].

Any alterations to the protocol requires prior submission and approval of an Event [Amendment].

Sincerely,

ANULIKA MBAKWE | ACC COORDINATOR
Department of Animal Care Services
Memorial University of Newfoundland
Health Sciences Centre | Room H1848
P: 709-777-6621
E-Mail: ambakwe@mun.ca